UNIVERSITY OF NAIROBI

CHARACTERIZATION OF THE TURKANA LOW-LEVEL JET STREAM AND THE ASSOCIATED RAINFALL USING CMIP6 MODELS AND ERA5 REANALYSIS

BY

OSCAR LINO

I56/16081/2018

A DISSERTATION SUBMITTED IN PARTIAL FULFILMENT OF THE REQUIREMENT FOR THE AWARD OF THE DEGREE OF MASTER OF SCIENCE IN METEOROLOGY OF THE UNIVERSITY OF NAIROBI.

JULY 2022

DECLARATION

I declare that this dissertation is my original work and has not been submitted elsewhere for examination, award of a degree or publication. Where other people's work, or my own work has been used, this has properly been acknowledged and referenced in accordance with the University of Nairobi's requirements.

OSCAR LINO Signature: 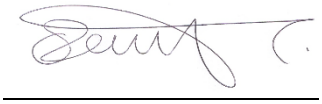 Date: Date: 04/July/2022…

I56/16081/2018

Department of meteorology

University of Nairobi

This dissertation is submitted for examination with our approval as research supervisors:

Dr. J.N Mutemi …….. Signature  Date: 04/July/2022…

Department of meteorology

University of Nairobi

P.O Box 30197-00100

Nairobi, Kenya

jnmutemi@uonbi.ac.ke

Dr. F.J Opijah…….. Signature 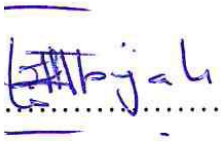 04/July/2022……

Department of meteorology

University of Nairobi

P.O Box 30197-00100

Nairobi, Kenya

fopijah@uonbi.ac.ke

DEDICATION

I would like to dedicate this work to my mother and late father, both who encouraged me to relentlessly pursue education and went out of their way to provide a background for my basic education. Their unwavering support gave me the craving for further education that I still hold up to today.

ACKNOWLEDGEMENT

The analysis in this work was done via JASMIN data cluster with datasets and resources supplied by the UK Met Office and other collaborators. We acknowledge efforts of the ECMWF of providing ERA5 datasets, and the World Climate Research Programme Working Group on Coupled Modelling, for providing CMIP6 datasets to support research. Special thanks to Joseph Mutemi and Franklin Opijah for guidance, suggestions and support during early stages of developing this work, Ellen Dyer for formatting and programming code for analysis and Thomas Webb for integrating the code into the UK Met Office Auto-Assess and publication on GitHub.

ABSTRACT

The Turkana low-level jet stream (TJ) is important to climatic conditions over northern Kenya and East Africa. The representation of the TJ in climate models varies due to the TJ interaction with Turkana channel that is influenced by model resolution and influences the model representation of the regional climate. This study compares features of the TJ in data from Coupled Model Intercomparison Project Phase 6 (CMIP6) model simulations with European Center for Medium-range Weather Forecasting atmospheric Re-Analysis version 5 (ERA5). The study presents analysis of spatial structure and annual cycle of the TJ, and relates strength of the TJ with topographic formation of the Turkana channel rainfall in the models and reanalysis (RA). Considering study period between 1981 and 2014, models reveal climatological wind speeds that match those of the reanalysis from the ERA5 at the jet entrance (13 m/s) but lower magnitudes of wind speed and vertical shears compared to ERA5 within the Turkana channel. The models with slowest wind speeds, have a flattened Turkana channel and fail to exhibit the terrain constriction at 37°E which otherwise aids in accelerating winds to form a jet core. Furthermore, they fail to represent the narrowing of the channel as in ERA5, thereby forming blocking walls in the channel, forcing vertical ascent and mixing, and weakening shear. This boosting of ascent motion promotes rainfall formation and enhances wet anomalies at the exit of the TJ when the jet stream is weaker. By applying a new narrowing index, we demonstrate the need to improve topography details in the CMIP6 models, particularly those with resolution coarser than 1.5°, in order to properly simulate the TJ and the observed rainfall over the northwestern areas of eastern Africa.

TABLE OF CONTENTS

ABREVIATIONS AND ACRONYMS

ACCESS-CM2	Australian Community Climate and Earth System Simulator coupled model, version 2
ACCESS-ESM1-5	Australian Community Climate and Earth System Simulator Earth System model
AMIP	Atmospheric Model Intercomparison Project
BCC-CSM2-MR	Beijing Climate Center, Climate System Model
BCC-ESM1	Beijing Climate Center, Earth System Model
CAMS-CSM1-0	Chinese Academy of Meteorological Sciences Climate System Model
CanESM5	Fifth Generation Canadian Earth System Model
CESM2	Community Earth System Model version 2
CMIP5	Coupled Model Intercomparison Project Phase 5
CMIP6	Coupled Model Intercomparison Project Phase 6
CNRM-CM6-1	Centre National de Recherches Meteorologiques Coupled Model version 6
CNRM-ESM2-1	Centre National de Recherches Meteorologiques Earth System model version 2
EALLJ	East Africa Low-Level Jet stream
ECMWF	European Center for Medium-range Weather Forecasting
ERA5	ECMWF atmospheric Re-Analysis version 5
ERA-Interim	ECMWF Re-Analysis -Interim version
FGOALS-f3-L	Flexible Global Ocean-Atmosphere-Land System, finite-volume version 3
FGOALS-g3	Flexible Global Ocean-Atmosphere-Land System, grid-point version 3

GFDL-CM4	Geophysical Fluid Dynamics Laboratory Climate model version 4
HadGEM3-GC31-LL	Hadley Centre Global Environment Model Global Coupled configuration 3.1, Low resolution
HadGEM3-GC31-MM	Hadley Centre Global Environment Model Global Coupled configuration 3.1, medium resolution
INM-CM4-8	Institute of Numerical Mathematics Climate Model
INM-CM5-0	Institute of Numerical Mathematics Climate Model
IPSL-CM6A-LR	Institut Pierre-Simon Laplace climate model low resolution
JJAS	June-July-August-September
JRA-55	Japanese 55-year Re-Analysis
MERRA2	Modern-Era Retrospective analysis for Research and Applications, version 2
MIROC6	Sixth version of the Model for Interdisciplinary Research on Climate
MPI-ESM1-2-HR	Max Planck Institute Earth System Model, High resolution
MRI-ESM2-0	Meteorological Research Institute Earth System Model, version 2
NCEP CFSR	National Center for Environmental Prediction (NCEP) Climate Forecast System Reanalysis
NESM3	NUIST Earth System Model (NESM) version 3
NorCPM1	Norwegian Convection Permitting Model version 1
NorESM2-LM	Norwegian Earth System Model, version 2
RA	Re-Analysis
SAM0-UNICON	Seoul National University Atmosphere Model Version 0 with a Unified Convection Scheme
TaiESM1	Taiwan Earth System Model 1.0

TJ	Turkana Jet stream
WCRP	World Climate Research Programme

LIST OF FIGURES

LIST OF TABLES

CHAPTER ONE

INTRODUCTION

1.1 Background of the study

Over northern Kenya, there exists a low-level jet stream which has great socio-economic potential for the region as well as being an important mechanism for moisture transport from the western Indian Ocean to some interior parts of northwestern East Africa (Vizy and Cook, 2019; Nicholson, 2014). This fast-flowing current of air, which is now called the Turkana low-level Jet stream (TJ), gained recognition among aviators who frequently experienced turbulence when landing and taking off from the region (Indeje *et al.*, 2001). The understanding of the TJ benefited from short field campaigns by Kinuthia and Asnani (1982) and Kinuthia (1992). The mean wind speeds in range 10 - 13 m/s culminate at 850 mb (Nicholson, 2016) in the year. Occasional ascents of pilot balloons during field campaigns in Kinuthia (1992) indicated the TJ is strongest during late night and early morning with associated wind speeds in range 30 to 50 m/s. The TJ is fragmented into two branches in the channel which merge at the mid-portion of the channel to form a jet core (Kinuthia and Asnani, 1982; Indeje *et al.*, 2001). Previous studies have related the TJ to the observed aridity over parts of Eastern Africa (Trewartha, 1981; Nicholson, 1996; Ba and Nicholson, 1998; Sun et al., 1999; Indeje et al., 2001; Nicholson, 2016). It is for this reason that the inclusion of the TJ in dynamical models is important to the representation of rainfall over the northern Kenya region (Sun *et al.*, 1999; Indeje *et al.* 2001; King *et al.*, 2021).

Eastern Africa (EA) is a generally dry region, found in an otherwise wet equatorial belt (Camberlin, 2018). The region is hyper-arid at the tip of the Horn and near the Egyptian border with annual rainfall below 150 mm (Njenga at al., 2014), an apparent extension of desert conditions from the bordering middle-East and Sahara respectively. An extensive area featuring less than 400 mm annual rainfall stretches from eastern Ethiopia through northwestern Kenya, to Lake Turkana (Nicholson, 2016; Camberlin, 2018). Extreme drought events have been common, exacerbated by climate systems that perturbs rainfall received, whose manifestations have increased notably since 2005. Between 2015 and 2016, drought prevailed over most parts of Ethiopia related to El Nino conditions (Sjoukje et al 2015), while 2016 and 2017 exhibited drought over the Greater Horn related to La Nina (Uhe *et al.*, 2015). Similarly, three drought events occurred in the seven years

alone (2005/2006, 2008/2009, 2010/2011) compared with only seven events in 30 years (1975 to 2004). The recent cyclicity in drought impacts has heightened interests in climate information from models to inform disaster risk management and increase people's adaptive capacity to climate extremes (Nicholson, 2014; Kilavi *et al.*, 2018).

Climate model information has led to understanding of the TJ and its influence on the climate in East Africa. Increased studies on the TJ using current generation of climate models and improved datasets can lead to a more quantitative understanding of the TJ as well as its impacts. The aridity is linked to regional topography and wind flow. Due to the north-south orientation of the east African highlands, advection of moist air from Congo-basin into the arid area is blocked (Slingo *et al.*, 2005). Lower-tropospheric (at 850 mb level) divergence matched by subsidence at mid troposphere characterizes the arid sub-regions (Yang *et al.*, 2015). The large-scale divergence is linked with the TJ as fast-moving winds cause drop in pressure due to Bernoulli effect (Indeje *et al.*, 2001) and interact with terrain within the channel, inducing frictional divergence (Ba and Nicholson, 1998). The divergence at lower atmosphere favors stable atmospheric conditions and dry climate over the plain and low plateau over coastal Tanzania, Kenya and Somali border, to the Nile plains of Sudan and South Sudan (Nicholson, 2016). The TJ also transports large amounts of moisture that promote rainfall formation at the jet exit in western parts of South Sudan and Ethiopia during the northern summer (Vizy and Cook, 2019). The strength of the TJ varies with large scale systems that drive rainfall over East Africa during October to December (Sun *et al.*, 1999; King *et al.*, 2021).

While the TJ is considered important to rainfall, some climate models such as the Community Atmosphere Model can exhibit weak low-level jet streams due to their low resolutions (Acosta and Huber, 2017). Climate models contributing to CMIP5 shows weaker TJ than in ERA5 during June to September months and comparable strength of the TJ in the remaining months of the year (King *et al.*, 2021). However, reasons for why the models represent the TJ the way they do, including the influence of the TJ on the airflow over the region, and how this affects the weather over the region in models, is not well understood.

1.1 Statement of the Problem

The TJ is important to climatic conditions over northern Kenya where it causes aridity and to northwestern East Africa where it is associated with rainfall through advection of moisture

Munday *et al.* (2020). The accuracy of model simulations of the climate over the Eastern African depends on how well the feature is simulated in the models. But, the representation of the TJ in climate models varies due to its interaction with topography over the Turkana area and the resolution of the model. A comparison of how several climate models simulate the TJ has been made in King *et al.* (2021) that shows that CMIP5 models have weaker zonal wind during northern summer and similar magnitudes of wind speeds as reanalysis (RA) datasets during northern winter. However, reasons for why the models represent the TJ the way they do, including the influence of the TJ on the airflow over the region, and how this affects the weather over the region in models, is not well understood. Through this study, an analysis was carried out to bring an in-depth quantitative understanding of the TJ characteristics using current generation of climate models.

1.2 Study Objectives

The overall objective of this study was to characterize features of TJ in the advanced CMIP6 models, understand how the features of the TJ might be related to topography in the models and how the differences in the model TJ might impact on the simulated rainfall.

To achieve the overall objectives above, the study involved the following:

1. Assessing how the TJ is characterized in current generation of climate models focusing on climatological location, and strength characteristics.
2. Determining how the TJ characteristics are influenced by the Turkana channel
3. Establishing extent to which varied representation of the TJ in the models affects how rainfall is simulated over north west of East Africa.

1.3 Research questions:

a) What are the climatic characteristics of the TJ in CMIP6 models?
b) How does the resolution and the representation of topography in the models be related to features of the TJ in CMIP6 models?
c) Is the simulated rainfall related to features of the simulated TJ?

1.4 Justification of the Study

This work focuses on characteristics of the TJ in CMIP6 models which are the latest generation of models available for us to study the climate in the past and anticipate future changes. It compares the characteristics of the TJ with the EAR5 that is optimized to give the best match to what would

be observed in observational data. Specifically, the study discusses model representation of the strength, structure and position of TJ along the Turkana channel whose varied representation with respect to observations may also induce biases in the simulated rainfall.

Model simulation of TJ features introduces a measure of uncertainty because of the lack of observational datasets. But since it is understood that some low-resolution models ignore low-level jet streams (Acosta and Huber, 2017), there is the opportunity to refine our understanding of the jet stream characteristics and influence on rainfall by using the recently available CMIP6 and ERA5 with high spatial resolution.

1.5 Significance of the Study

The ERA5 leverages on continuous development process that forecast models have undergone and to offer higher spatial and temporal resolution in reanalysis, historical climate products. Development in modeling is a continuous process and whereas better products are getting available, there is the need to understand model uncertainties and build confidence in them. Through evaluating the model representation of a key feature to rainfall in the region, this study informs both model development process and model use as argued in James *et al.,* (2017).

1.6 The Study Area

East Africa encompasses varied terrain, characterized by elevation gradients ranging from the highest elevation point at 5, 395 m above mean sea level (Mount Kilimanjaro) to the lowest elevation point of 153 m below mean sea level, in Djibouti. This culminates in a north-south organization of elevated terrain (Figure 1) that separates East Africa into two regions.

The Ethiopian highlands (Ethiopian Massif) are the most expansive (McCann, 1995) with about 50% if it elevated above 1,500 m above mean sea level. The highlands are characterized by a mixture of tablelands, valleys and several summits elevated at about 4,000 m above mean sea level. The Turkana channel boarders the Ethiopian highlands to the south and characterizes the low elevation terrain over northern Kenya. Other highlands extend from Kenya-Uganda boarder to central Kenya with a terrain gap that intercepts the Kenya-Uganda boarder to central Kenya high terrain elongation, known as the Rift Valley. Kenyan highlands peak at Mount Kenya with an elevation of 5,199 m above mean sea level. In Tanzania, Mount Kilimanjaro protrudes with an elevation of 5,895 m and in Uganda, Mount Elgon is elevated at 4,321 m above mean sea level.

To the west of the Kenyan highlands, lays a fairly flat expanded elevation at about 1,000 m that contains Lake Victoria.

Regions around the equator on the globe are generally wet, although other areas are wetter than others induced by varied topography. The wet climate supports tropical rain forests which are characterized by lofty trees and dense undergrowth. However, the climatic conditions of East Africa do not support such growth that otherwise proceed throughout the year without seasons. Parts of the East African region which are to the west of the Nile valley exhibit a peak in rainfall season during the boreal summer of June-July-August (JJA) and those to the east showing bimodal regimes; the March-April-May (MAM) long rain and the September-October-November (SON) short rain seasons (Nicholson, 2018). The rainfall seasons shifts back to a unimodal regime further to the south, that peak when the season is summer in the southern hemisphere; December-January-February (DJF). The rainfall regimes are largely attributed to the North-South movement of trade winds convergence zone (Henderson *et al.,* 1949; Miller 1971).

The East Africa is hyper-arid at the tip of the Horn of Africa and near the Egyptian border with annual rainfall below 150 mm (Njenga at al., 2014), an apparent extension of desert conditions from the bordering middle-East and Sahara respectively. An extensive area featuring less than 400 mm annual rainfall stretches from eastern Ethiopia through northwestern Kenya, to Lake Turkana (Nicholson, 2016; Camberlin, 2018).

The aridity exhibited to the east of the north-south oriented East African highlands is related to the wind that is associated with TJ whose flow is divergent. The west of the East African highland is wetter due to the influence of the zonal winds from the Congo Air Boundary (Howard and Washington 2019). The zonal advection of the moisture-laden wind from the Congo basin to the drier east is impeded by the terrain barrier (Slingo *et al.,* 2005).

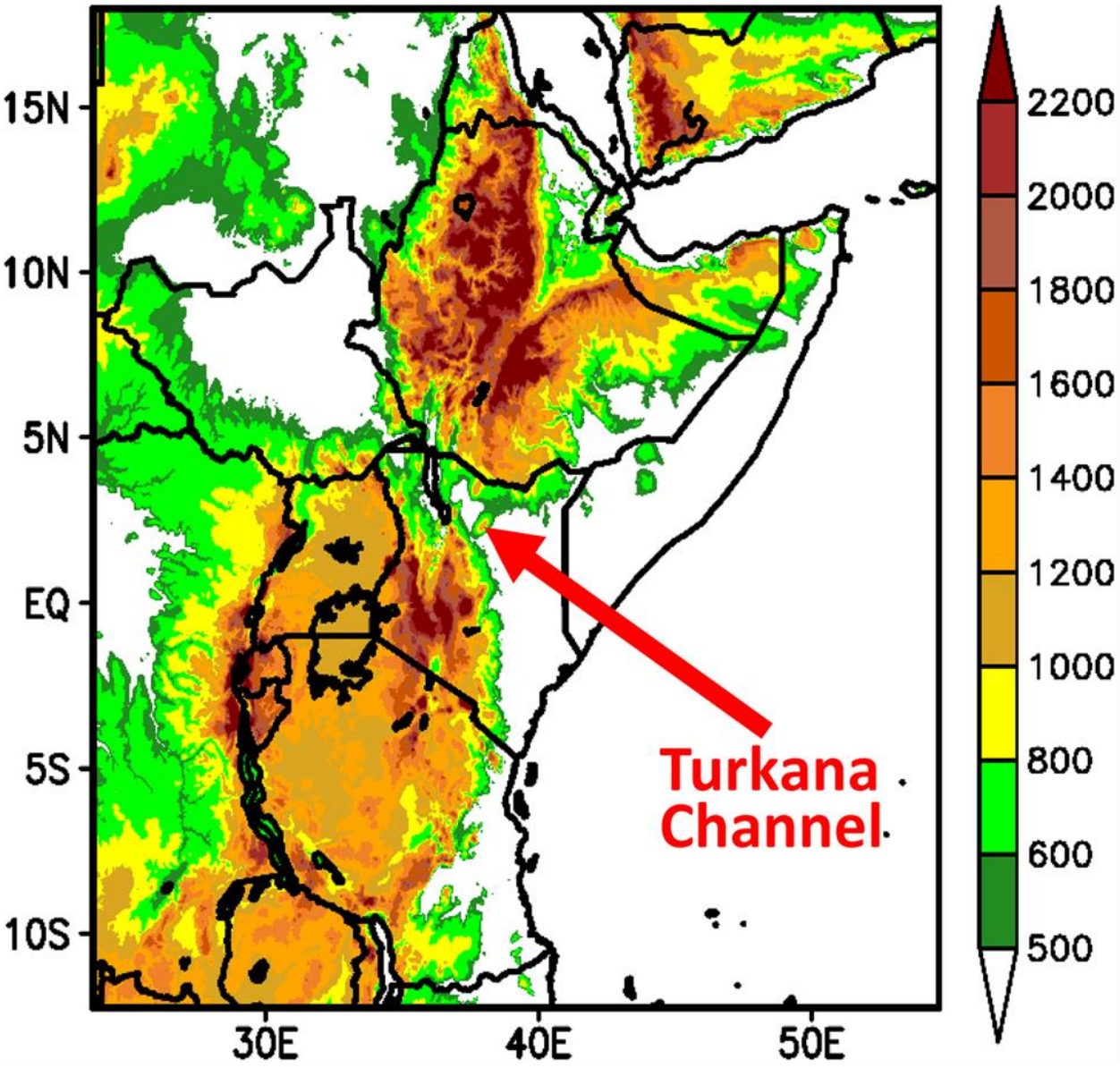

Figure 1. *Map of East Africa showing the boundaries, terrain (meters above sea level), (Source; Vizy and Cook, 2019)*

CHAPTER TWO

LITERATURE REVIEW

2.1 Introduction

This chapter describes in detail the previous studies related to the formation, maintenance and characteristics of the TJ. The section also revisits literature that link the TJ with the rainfall in East Africa.

2.2 Known mechanism of formation and maintenance of Low-level jet streams

There exist several areas of the lower atmosphere with relatively fast winds known as low-level jet stream such as in North America (Parish and Olman, 2010), South America (Repinaldo *et al.*, 2015), East Asia (Wang *et al.*, 2011), West Africa (Nicholson and Webster, 2007) and East Africa (Rai *et al.*, 2018).

Mechanisms which often lead to their existence include orographic channeling of low-level winds that lead to their acceleration through narrow terrain gaps (Liu *et al.*, 2000; Washington *et al.*, 2006; Holbach and Bourassa 2014). Inertial forcing from cross-equatorial transport of planetary vorticity has also been shown to induce horizontal shear in wind speeds in the EALLJ (Hart, 1977) and the African Westerly Jet stream (Nicholson and Webster, 2007; Pu and Cook, 2010) in Africa. Low-level jet streams can also occur as a result of frictional interaction with ageostrophic flow associated with upper-level jet streams such as over the Great Plains (Parish and Oolman, 2010).

Among low-levels jet streams, there are those that form on continental regions while others are observed over coastal areas, and they mainly differ in the way the fast-traveling winds are maintained. The low-level jet streams in continental interiors are usually sustained through constriction of winds when traveling through channels between adjacent elevated terrain, inertial forcing resulting from cross-equatorial wind flow and secondary effect of ageostrophic circulations in the vicinity of upper-level jet stream (Parish, 2000).

On the other hand, coastal low level jet streams have been associated with acceleration of winds that are in geostrophic balance; being controlled by balance between the forces of Coriolis and pressure gradient that is induced by land-sea temperature contrasts on daily time scale (Jiang *et*

al., 2010). Such low-level jet streams exist along coastal regions of Chile (Munoz and Garreaud, 2005), over the coast of California (Cook and Vizy, 2010), the African Westerly along the south of west African coast (Pu and Cook, 2010; Nicholson, 2010).

In the East African region, a low-level jet stream (EALLJ) forms at the coastal Somali (Hart, 1977). The EALLJ forms as a result of cross-equatorial northerly advection of planetary vorticity that is directed to the east coast of Africa by the north-south barrier highlands of East Africa.

2.3 Known features of the TJ and the TJ connection with the Turkana channel

While low-level jet streams in the continental interior are majorly associated with channeling of winds by the terrain, there have been different ways that the winds have been shown to interact with the topography to form a low-level jet stream. Some low tropospheric jet streams have been shown to result from the acceleration of winds that is guided by balance between the forces of Coriolis and pressure gradient that is induced by nighttime cooling over elevated terrain that has a sloped orography. The jet streams eventually flow parallel to slope contours, such as the South American low-level jet stream (Wang and Fu, 2004) and the low-level jet streams in Gulf of California (Anderson *et al.*, 2001). Elsewhere, some low-level jet streams in the interior continent have been shown to follow the channeling of winds through gaps between adjacent elevated terrain with sloped orography as large scale induced inland flow drifts through such an orographic orientation. Such low-level jet streams include the Bodélé Jet stream in eastern Sahara (Washington *et al.*, 2006), low-level jet streams in central Iran (Liu *et al.*, 2000), and the TJ in East Africa (Indeje *et al.*, 2000; Nicholson 2016).

Since the TJ stream was first documented following pilot-balloon observations by Kinuthia and Asnani (1982), there has been efforts to understand features of the jet stream. For instance, the jet exists in a 700 km long valley that lies between the Ethiopian highlands and Kenyan highlands (Kinuthia and Asnani, 1982; Kinuthia, 1992). These fast-traveling winds accelerate at the narrowest area within the channel, near Marsabit and eventually decelerate when the winds get to wider areas of the channel north-western Turkana region (Kinuthia 1992). The TJ achieves core wind speeds of about 13 m/s within 650 to 930 millibar pressure levels (Indeje *et al.*, 2001).

The TJ is prominent whenever there is monsoon flow that blows in south easterly during May to September months (boreal summer). During the Indian monsoon, high speed winds are exhibited

at entrance of the Turkana channel when the strong southwesterly EALLJ is also present (Boos and Kerry, 2009). The EALLJ extends over coastal and eastern parts of East Africa (Anderson 1976; Krishnamurti *et al.*, 1976; Hart *et al.*, 1978, Bannon 1979, Boos and Kerry, 2009).

Since the TJ is formed and sustained by monsoon background flow rushing through the Turkana channel, it could be modulated by strength of the background flow on annual timescale and the formation the Turkana channel constriction in the long term (Indeje *et al.*, 2001). Ba and Nicholson (1998) indicate that on daily time scales, intensification of slope winds related to mesoscale circulations induced by convective activities happening further to the west over Lake Victoria coincides with variability in strength of the TJ. Nicholson (2016) also indicates that ascends from mesoscale circulations over elevated terrain closer to the TJ coincides with peak TJ strength. Therefore, there is an apparent diurnal cycle in the TJ.

Ascends and descends dominate over areas of slopped terrain under when synoptic conditions are weak (Catalano and Cenedese, 2010). The slope winds are primarily forced by either thermal contrasts that lead to pressure forces that drive airflow along the gradient, and/or effects of friction that causes airflow to be directed into ascent whenever the rushing air interacts with elevated terrain. Hence, they play a critical role in modulating profiles in layers of the atmosphere (such as wind, moisture and thermal) and therefore, can influence the structure and strength of a low-level jet stream.

2.4 Influence of the Turkana Jet stream on regional climate

Eastern Africa (EA) is a generally dry region, found in an otherwise wet equatorial belt (Camberlin, 2018). The region is hyper-arid at the tip of the Horn and near the Egyptian border with annual rainfall below 150 mm (Njenga at al., 2014), an apparent extension of desert conditions from the bordering middle-East and Sahara respectively. An extensive area featuring less than 400 mm annual rainfall stretches from eastern Ethiopia through northwestern Kenya, to Lake Turkana (Nicholson, 2016; Camberlin, 2018). The highland areas receive much enhanced rainfall, with mean annual rainfall ranging between 600 to 1200 mm, associated with orographic rainfall. Over northwest part of East Africa and Ethiopian highlands, major rainfall season peak is observed during northern summer which is also the peak of West African monsoon season (Levin *et al.*, 2009; Williams *et al.* 2012; Mekonnen and Thorncroft 2016).

The aridity over most parts of the regions is linked to regional topography and wind flow. Due to the north-south orientation of the east African highlands, advection of moist air from Congo-basin into the arid area is blocked (Slingo et al., 2005). Lower-tropospheric (at 850 mb level) divergence matched by subsidence at mid troposphere characterizes the arid sub-regions (Yang et al., 2015). The large-scale divergence is linked with the TJ as fast-moving winds cause a drop in pressure due to Bernoulli effect (Indeje et al., 2001) and interact with terrain within the channel, inducing frictional divergence. The divergence in the lower atmosphere leads to formation of stable atmospheric conditions, resulting into a shallow moist layer and a dry climate over the Turkana channel and its flanks including Kenya and Somali border, the Nile plains of Sudan and South Sudan (Trewartha, 1981; Ba and Nicholson, 1998; Nicholson, 2016). The TJ also transports moisture that promote rainfall formation at the jet exit in western South Sudan and Ethiopia and shifts rainfall regime from eastern South Sudan during the northern summer (Vizy and Cook, 2019). The strength of the TJ covaries with the ENSO system that drives rainfall over East Africa during October to December (Nicholson, 1996; Sun et al., 1999; King et al., 2021).

2.5 The TJ and the East African Rainfall in climate models

Acosta and Huber (2017) attribute the ability of the Community Atmosphere Model over the Indo-Gangetic Plain to correctly simulate low-level jets to proper representation of model physics schemes that explicitly resolve the Indo-Asian monsoon. Using a grid resolution of 0.5°, Indeje *et al.*, (2001) reported a fairly good representation of the features in the TJ compared with the observations in Kinuthia (1992), using the National Center for Atmospheric Research (NCAR) model. A comparison of how several climate models simulate the TJ has been made focusing on annual cycle and interannual variability of the TJ in CMIP5 (King *et al.*, 2021). While in the seasonal cycle the TJ is strong during the two major rainfall seasons in East Africa (March to May and October to December), its strong anomalies are accompanied by dry conditions in its area of influence. Munday *et al.* (2020) suggests that the CMIP5 models with horizontal resolution of more than 60 km do not replicate the associated dry anomalies as finer grid lengths are required to accurately simulate the TJ and its interaction with East African climate.

While the October to December and March to May seasons are of great importance to most parts of Eastern Africa that are generally wet, climate models which predict future situation of the region with regards to rainfall, still exhibit biases in their information for the region. For instance,

historical model simulations by coupled models contributing to phase 3 and 5 of the Coupled Model Intercomparison Project (CMIP 3 and CMIP 5) shows the models overestimate rainfall in East Africa in the October to December short rain season and underestimate it during the March to May long rain season in East Africa (Yang *et al.*, 2015). The reason for these biases were attribute to large-scale forcing of sea surface temperatures and smoothing out of localized features specific to East African climate. Similarly, a study by Ongoma *et al.*, 2017 on CMIP 5 show the model projections capture the bimodal rainfall regime that is prevalent in East Africa, but they similarly overestimate rainfall in the October to December short rain season and underestimate it during the March to May long rain season in the region. They indicate that in the models, rainfall in African continent is likely to increase due to being forced by localized mesoscale circulation from features within East Africa such as the Lake Victoria and the East African highlands. They conclude that the projected changes in rainfall are likely to have larger biases in climate models of coarse resolution that parameterizes important features to climate in the region.

The reasons for why the models represent the important TJ, the way they do including the influence of the TJ on the airflow over the region, and how this affects the weather over the region in models, is not well understood. Furthermore, there have been no previous studies of the simulation of the TJ in the newest generation of global models.

2.6 Conceptual framework used in the study

The schematic flow chart (Figure 2) shows interlinkage between the input data from ERA5 data and CMIP6 model to summary outputs through objectives of the study. This characterized the TJ in CMIP6 models and compared with the TJ characteristics in ERA5 that represent observations. The Turkana channel influences the TJ by constricting the low-level winds and therefore, how well the climate models represent the narrowing in the channel, determines TJ strength and structure in them. The channel shape was determined in the datasets and linked with the TJ strength to assess how the Turkana channel influences the TJ. Models with TJ of varied strength were analyzed to establish how the fluctuations in the strength influences rainfall anomalies in the model. The TJ characteristics in CMIP6 models were therefore determined and associated rainfall anomalies quantified.

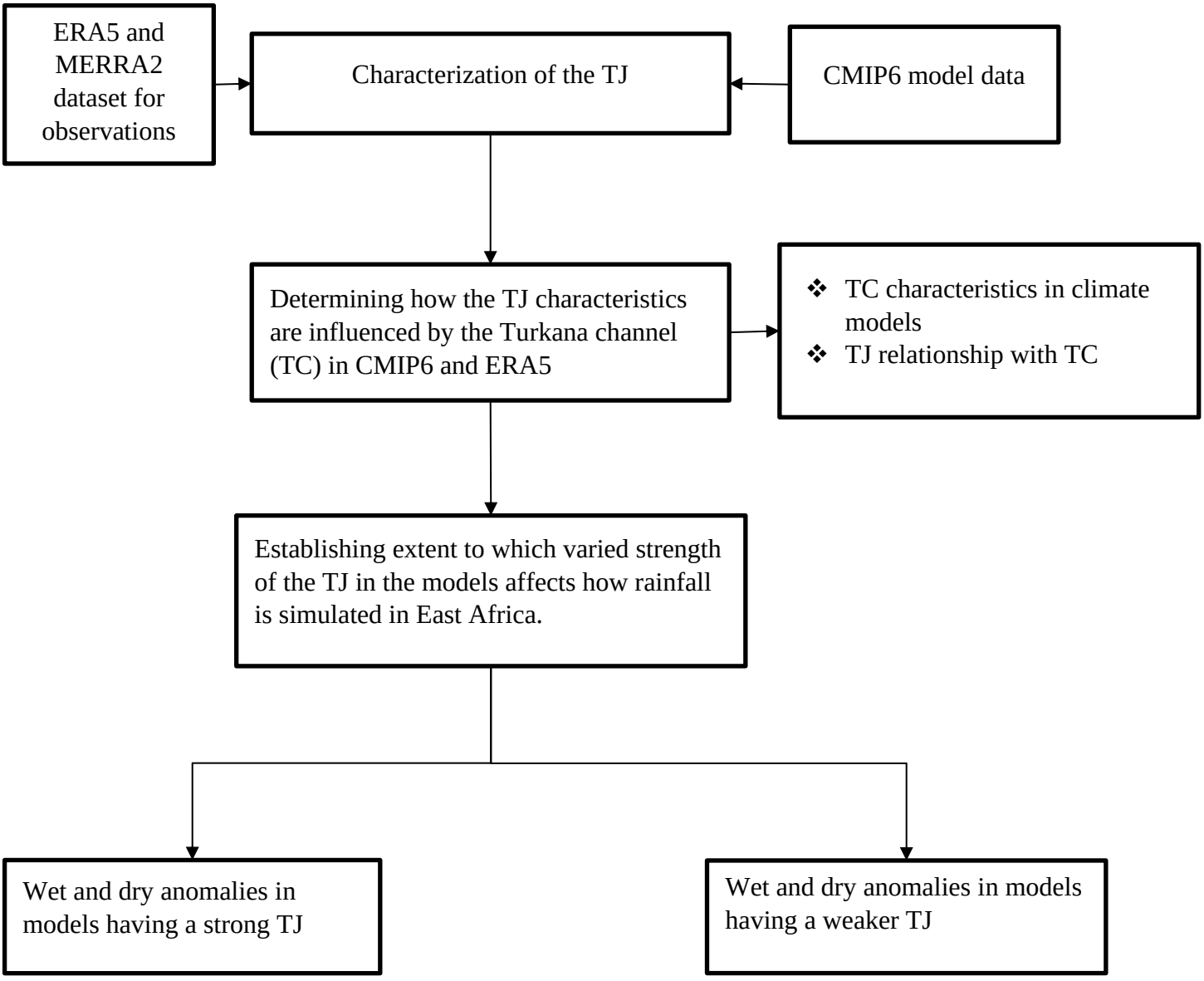

Figure 2. *A schematic showing of key elements referred to in this work. The high-resolution RA datasets are used to characterize the TJ into strong/weak and a framework for linkage to the Turkana channel is built. The anomalies associated with a strong/weak TJ which quantifies how missing the TJ in the models, contributes to biases in rainfall in the region.*

CHAPTER THREE

DATA AND METHODS

3.1 Introduction

This chapter describes in detail the materials and methods used to realize the objectives of the study. It details the climate model data, RA and observational data use. The methods of quantification of strength, location and associations with topography are also discussed.

3.2 Datasets

This study makes use of the data from the sixth iteration of the Coupled Model Intercomparison Project (CMIP6; Eyring et al., 2016) under the World Climate Research Programme (Taylor et al. 2012). The historical Atmospheric Model Intercomparison Project (AMIP), which is one of the four baseline experiments from CMIP6, were considered for a period between 1980 to 2014. Twenty-six atmospheric models (Table 1) were analyzed, which were the models with all variables needed for this analysis. The historical AMIP runs were chosen for this analysis as they assume the historical sea surface temperature (SST) input into the experiments. Consequently, they may reduce uncertainties related with SST feedback (Eyring et al. 2016) and allow for oscillations in the output data to be matched with the atmospheric reanalysis datasets. The resolution of the models differs but the analysis was performed on the models' native grid to preserve the original information. Among the models used, 4 were drawn from the High-Resolution Model Intercomparison Project (HighResMIP) and 22 were regular experiment models. HighResMIP models are designed to represent climate processes with global model resolutions (~25 km). HighResMIP models used in this study included HadGEM3-GC31-MM, MPI-ESM1-2-HR, IPSL-CM6A-LR and CNRM-CM6-1.

To benchmark the findings by the models, this study takes advantage of the latest reanalysis dataset from the fifth version of European Centre for Medium-Range Weather Forecasts reanalysis - ERA5 (Hersbach et al., 2019). In ERA5, the 2000 to 2017 climatological wind speeds associated with the TJ matches well with structures found using NCEP CFSR reanalysis dataset (Hartman 2018), and MERRA2 dataset although the TJ is stronger in MERRA2 during early months of the year (Vizy and Cook 2019). However, the climatological wind speeds in the ERA5 are comparable, albeit slower than 31 m/s that was occasionally recorded in the July 1979 to June 1980 single year

of field observations in Kinuthia (1992). This disparity is hypothesized to be as result of terrain features of smaller scale that are not resolved in the reanalysis at the horizontal resolution of 0.25°.

Table 1: Name and description of CMIP6 models used in this study. Marked 1 are models from the High-Resolution Model Intercomparison Project (model run at ~ 25 km or finer). Marked 2 are models run at higher grid resolutions

MODELING CENTER	MODEL	Atmospheric horizontal resolution (°)
AS-RCEC	TaiESM1[2]	0.94×1.25
BCC	BCC-ESM1[2]	1×1.25
	BCC-CSM2-MR[2]	0.94×1.25
CAMS	CAMS-CSM1-0[2]	0.94×1.25
CAS	FGOALS-g3[2]	1.39×1.41
	FGOALS-f3-L[2]	1.39×1.41
CCCma	CanESM5[2]	1.39×1.41
CNRM-CERFACS	CNRM-CM6-1[1]	0.56×0.83
	CNRM-ESM2-1[2]	1.25×1.88
CSIRO	ACCESS-CM2[2]	1.25×1.88
	ACCESS-ESM1-5[2]	1.25×1.88
INM	INM-CM5-0[2]	5.18×2
	INM-CM4-8[2]	1.85×1.88
IPSL	IPSL-CM6A-LR[1]	1.11×1.13
MPI-M	MPI-ESM1-2-HR[1]	1.11×1.13
MIROC	MIROC6[2]	1.5×2
MOHC	HadGEM3-GC31-LL[2]	1×1.25
	HadGEM3-GC31-MM[1]	0.93×0.94
MRI	MRI-ESM2-0[2]	1.11×1.13
NCAR	CESM2[2]	1.89×2.5
NCC	NorESM2-LM[2]	1.27×2.5
	NorCPM1[2]	1.89×2.5
NOAA/GFDL	GFDL-CM4	0.94×1.25

NUIST	NESM3[2]	2.77×2.81
SNU	SAM0-UNICON[2]	2.77×2.81

3.3 Methods

The analysis principally aims at describing the following elements of the TJ in CMIP6 models: range of values for maximum winds, seasonal cycle of the TJ, its spatial structure, the detection threshold of the TJ, the narrowing index (representing shape of the Turkana channel), and the precipitation index quantifying extent to which varied representation of the TJ in the models affects rainfall in East Africa

3.3.1 Characterization of the TJ in climatology

3.3.1.1 Annual cycle

The seasonal shift in the direction of the TJ is determined by assessing the prevailing wind vectors over East Africa, which shift direction from southerly to northerly, following the apparent movement of the overhead sun in a year. The horizontal extent of the TJ was identified in both the RA and models by masking the mean wind for speed of magnitudes less than 5 m/s. the 5 m/s threshold represented wind speeds for areas within the Turkana channel in the RA datasets. The resultant wind vectors at the 850 mb level provided a key map showing the relatively high-speed winds with an axis confined within the Turkana channel in ERA5 and most of CMIP6 models. This matched the observational work of Kinuthia and Asnani (1992) who reported that the TJ culminates in the layers 925 and 700 mb with wind speeds of about 13 m/s within the Turkana channel.

3.3.1.2 Location of the TJ

The location and structure of the TJ is determined in vertical wind profiles for the cross section through the Turkana channel, which is at the point 2°S, 43°E to the point 8°N, 32°E. Those points were used by Nicholson (2016) to mark the cross-sections. In this work, the TJ exit coincided with a point beyond which the wind decelerated rapidly. The winds accelerate in the mid-portion of the Turkana channel particularly in October to May season depicting a jet core. Finally, the jet entrance marked the point of entry of winds into the Turkana channel.

3.3.1.3 TJ detection threshold

The threshold of the occurrence of the TJ was identified when the structures of the cores of the TJ in the model matched those in the ERA5 datasets. A search criterion was applied to the wind speed at 37°E, 3°N for mean JJAS seasons over the period of 35 years to identify optimal thresholds for a strong and well-formed TJ. Thresholds for maximum winds at 850 mb level were searched in range 6 m/s and 12 m/s, along with thresholds for wind shears in range 2 m/s and 6 m/s. Shear was taken to be the difference between maximum wind speed at 850 mb and minimum wind speed found at any level above the 850 mb, searching before 500 mb level is reached. The Optimum thresholds of maximum wind speed and shear for the TJ during JJAS in the models is that which the majority of the models, especially those of higher resolution with a well-formed Turkana channel (described by index of narrowing) that maintains it. The thresholds applied in studying the TJ using ERA-Interim dataset of maximum wind speed 10 m/s, matched with decreasing wind speeds aloft in 2-4 m/s (Nicholson, 2016) and those postulated by Oliviera et al., (2018), were found too stringent to capture a TJ in the models.

3.3.2 TJ connection with the Turkana channel

3.3.2.1 Vertical motion (Omega)

The omega is used to assess the TJ interaction with the topography in the Turkana channel through mean flow. The mean omega values are extracted for a transect through the Turkana channel (point; 2^{o} S, 43^{o} E to point; 8^{o} N, 32^{o} E). Those points were used in Nicholson (2016) to mark the cross-sections. In this work, the jet exit coincided with a point beyond which the wind speeds diminish rapidly. The winds accelerate in mid-portion of the Turkana channel particularly in October to May season depicting a jet core. Finally, the jet entrance marked the point of entry of winds into the Turkana channel. Values from this analysis indicate a tendency of the wind to flow either upwards or downwards across the three regions in the Turkana channel.

3.3.2.2 Narrowing Index

The TJ is associated with topography through the shape of the Turkana channel. The shape is described using the narrowing index estimated as the mean change in the cross-sectional area of the channel. The cross-sectional area was obtained by estimating the area under a curve between constant 850 mb and the surface below the pressure level along a longitude. The cross-sectional area was calculated along each longitude for the longitudes 33°E (marking the exit of the jet stream)

to 42°E (marking the entrance of the jet stream), and bounded by the latitudes 2°S and 9°N. The Turkana channel is the largest topographic feature below the 850 mb level, with floor at 700 m (Camberlin, 2018) within the domain bounded by those coordinates. The narrowing index summarizes the consistency in narrowing towards the constriction at the mid-portion of the Turkana channel, and indicates the relative ease of air mass to flow through the channel without being blocked and being accelerated to form an intense TJ core in accordance with Bernoulli's principle (Indeje et al., 2001).

3.3.2.3 Spearman's rank correlation

The association between the Narrowing in the Turkana channel and model resolution as well as the association between TJ and the Turkana channel, are quantified using the Spearman's rank correlation. The narrowing index is correlated with the model resolution. Since the x and y grid step sizes were not uniform, the model resolution was taken to be the grid-step size in x-direction instead of computing the grid area. This is because the grid-step size in x-direction was in the same order with the narrowing index. The narrowing index was correlated with the TJ count to test significance of association between the narrowing index and the TJ strength in the models. Since the TJ was found to be stronger in most models when thresholds considered are lowered (in comparison to those used previously using RA datasets), the relationship is skewed towards this, making the Spearman's rank correlation an appropriate method as used in Vizy and Cook (2019).

3.3.3 TJ influence on rainfall

3.3.3.1 Precipitation Index

A precipitation index is computed for climatological precipitation associated with the TJ in CMIP6 models. The index is obtained by averaging the seasonal rainfall during TJ occurrences. These TJ events were isolated from the 35 years of analysis by identifying when the core wind speeds in the TJ reached the detection threshold of the TJ which were achieved during JJAS season. This season matches when moisture is high at the TJ exit region as it is the main rainfall season over the north-western parts of East Africa (Camberlin 2019).

3.4 Assumptions and limitations

By using atmosphere only model simulation, this work ignores possible variability of the TJ attributed to Sea Surface Temperatures (SST) feedback. This consideration is likely to have

overlooked the possible long-term weakening of the TJ found in 3 RA datasets (King *et al.*, 2021) which is postulated to result from TJ interaction with Walker Circulation system driven SSTs. The use of the atmosphere only simulations was necessary to limit the analysis to TJ variability related to the interaction with land surface and also constrain the study from further uncertainties from SST feedback.

CHAPTER FOUR

RESULTS AND DISCUSSION

4.1 Introduction

This chapter presents results from analysis of various aspects of the TJ. The climatological strength, location and structure of the TJ is characterized in CMIP6 models and the ERA5. The structure and strength of the TJ is also associated with the shape of the Turkana channel. Rainfall anomalies is also associated with the TJ strength in this chapter.

4.2 Characteristics of the TJ

4.2.1 Seasonal cycle of the TJ in CMIP6 model climatology

The mean wind speeds for 1980 to 2014 are shown for a point at mid Turkana channel (Figure 3). In ERA5 and MERRA2, they remain relatively high throughout the year with mean values ranging between 10 and 13 m/s. The MERRA2 emphasizes on existence of a peak in March and higher one in September, which is also exhibited in ERA5, matched by a low in July. In different reanalysis (MERRA2, ERA5, and JRA-55) datasets, the TJ has similar peak and low seasons although with a bias from each other (Vizy and Cook, 2019; Kings et al., 2021). While TJ strength is similar in September, stronger in MERRA2 March, and weakest between April and October in JRA-55, among the three datasets (Kings et al., 2021).

The HadGEM-GC31 models similarly have about a 2 m/s range between maximum to minimum values as depicted in ERA5 and MERRA2, albeit the peak and low magnitude of the models is lower. Most variation between the different CMIP6 models is exhibited between May and October. In this period also, the spread of individual model values about the ensemble is minimal, indicating that most of the models agree. Despite this agreement, they do exhibit relatively lower values compared with reanalysis data. During the same months, the BCC-ESM1 model exhibited categorically low mean wind speeds, ranging between 5 and 9 m/s with particularly low values from April to September. While it has been suggested that model resolution can determine the TJ representation (Indeje et al., 2001), this result shows that at similar resolution to HadGEM-GC31-

LL, the TJ in BCC-ESM1 (see table 1) is weaker with different seasonal cycles. This work explores what might be the drivers for these differences.

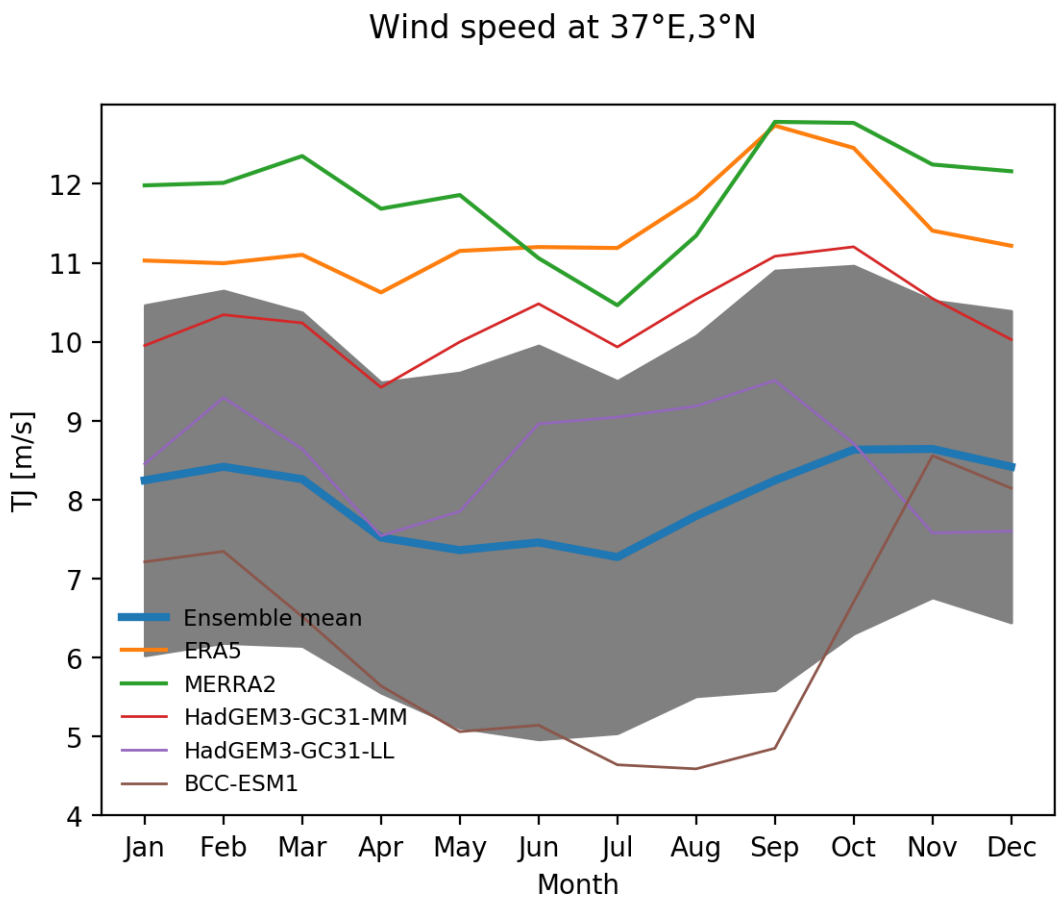

Figure 3. *The 1980 to 2014 mean wind speeds in reanalysis datasets (ERA5 and MERRA2), three CMIP6 models (HadGEM3-GC3-MM, HadGEM3-GC3-LL and BCC-ESM1) and the 26 CMIP6 model (shown in Table 1) ensemble at the 850 mb level in each month of the year for the grid closest to 37°E, 3°N (green dot shown in Figure 2). Gray shaded region denotes the range of values for climatology in CMIP6 models (computed as +/- one standard deviation of the 26 models in each month around the ensemble mean).*

Presence of the TJ in a year is investigated by masking wind vectors for winds speeds below 5 m/s at 850 mb level. The pressure level is chosen since the wind here flows above the terrain and therefore, it is the lowest level of the TJ which is free from obstruction by the terrain barrier. Figure

4 (panels a to b) to compare the mean wind vectors in ERA5 versus wind from 2 CMIP6 models (HadGEM-GC31-LL and BCC-ESM1). High wind speeds of at least 5 m/s in both ERA5 and the HadGEM-GC31-LL throughout the year, are constrained within the Turkana channel. The BCC-ESM1 model has the winds spread out over Kenya.

In a single year, the prevailing wind direction shifts from southerly during May to September, to northerly during October to April. There is splitting of the flow into two streams of south-easterly flow (TJ) and to a larger extent, a south-westerly flow (East Africa Low Level Jet- EALLJ) over northern Kenya that is pronounced during the May to September season. This splitting is first seen in the year, in May as evident in figure 3a and 3b (May panel in ERA5 and the HadGEM-GC31-LL). The north-easterly stream forms the TJ with a clear axis from southeast to northwest in April through October in both the ERA5 and the HadGEM-GC31-LL model.

The wind speeds are shown for a point at mid Turkana channel. In ERA5, they remain relatively high with mean values ranging from 11 m/s in January through July to 13 m/s in September (ERA5 panel in figure 4d). Similarly, the HadGEM-GC31-LL model has a 2 m/s range between maximum to minimum mean values as the highest values are exhibited in September. However, the values in the HadGEM model are of magnitudes ranging between 8 and 10 m/s. The BCC-ESM1 model revealed a further lower magnitude of wind speeds ranging between 5 and 9 m/s with particularly lowest values in presence of the EALLJ, from April to September.

The Southerly winds carry moisture into the region during northern summer time compared to other months of the year (figures 4a to 4c). The southerly flow has its sources in the sources in the ocean, hence it is laden with more moisture compared to other months when the flow is northerly. The reanalysis and the HadGEM-GC31, having relatively stronger TJ as previously discussed, are indicating higher moisture fluxes during period. In the BCC model, high wind speeds at the entrance, do not extend to mid-Turkana channel as far as HadGEM winds do (Figure 4). The analysis also indicates that BCC wind speeds drop off more than HadGEM in climatology and therefore, moisture fluxes in the BCC is lesser in Figure 4d. This period coincides with when the regions bordering the northwest of Kenya receives extended rainfall (Chamberlin, 2018). Considering the TJ is a major transporting agent for moisture into northwest of East Africa (Vizy and Cook 2019; Munday et al., 2020), simulated impacts of the TJ to rainfall are likely to be different in the reanalysis and in the CMIP6 models that show a weaker TJ during the season.

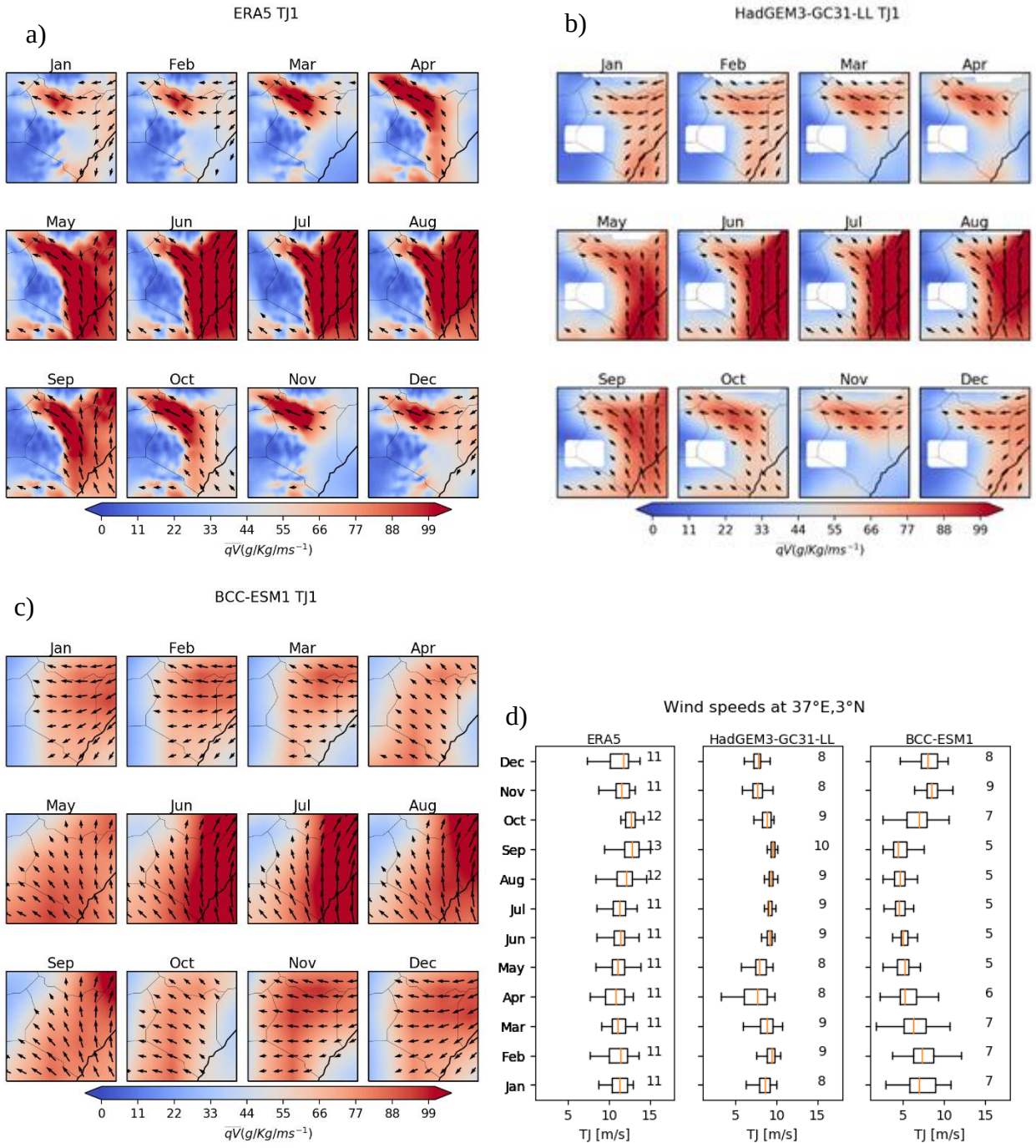

Figure 4. *Mean monthly moisture flux at 850 millibars (g/Kg/m/s), overlaid with mean wind vector at 850 millibars (m/s) for different datasets in plots a, b and c. Wind vectors indicate winds of at least 5 m/s. In plot d, are box and whiskers for wind speed at the same level in each month of the year for the grid closest to 37^o E, 3^o N. Inserted values in plot d, are mean values for each month*

4.2.2 Spatial Structure in climatology of the TJ in CMIP6 models

The mean vertical structure of the lower atmosphere (surface to 500 mb pressure level) winds is analyzed along the Turkana channel in CMIP6 models (figure 5). In the ERA5 as well as in the models, the relatively high-speed winds are located above the surface; wind speeds increase between the surface and 850 mb and decrease with altitude increase. The center of intensity appears between 925 mb and 850 mb pressure levels near the middle of the Turkana channel following acceleration at this point (Patwardhan and Asnani, 1999; Indeje *et al.*, 2001).

At the mid-Turkana area, the ERA5 and both versions of the CNRM model exhibit the highest change in wind speeds from maximum (approximately 12 m/s) at 850mb to minimum (approximately 7 m/s) before 500 mb level is reached in JJAS season (figure 5a). Other models with relatively high changes from maximum to minimum wind speed at higher pressure levels of more than 5 m/s during this season include HadGEM3-GC31-MM, MRI-ESM2-0, CESM2, FGOALS-f3-L, SAM0-UNICON, ACCESS-CM2, HadGEM3-GC31-LL, IPSL-CM6A-LR and CanESM5. The rest of the models show lower changes as mean winds are slower at the mid-Turkana channel. They show the center of intensity further away from the middle area of the Turkana channel. The models are namely BCC-ESM1, CAMS-CSM1-0, SAM0-UNICON, TaiESM1, MIROC6, NESM3, INM-CM4-8, and INM-CM5-0. In them, high wind speeds that fail to extend up to mid-Turkana Channel, an apparent consequence of the TJ merging with the EALLJ during the JJAS season.

During the October to May months, the EALLJ is absent, the center of intensity in the wind speeds shifts northwards to mid-channel area, it is elevated, has a vertical elongation up to about 825 mb (figure 5b). As the winds flow through the channel in absence of the EALLJ, they are displaced upwards by the gently rising slope indicated in topography below each panel. The vertical extension of the TJ core is accompanied by weaker changes from maximum to minimum wind speeds during the October to May months. The weakening appears pronounced in a set of models which exhibited the center of intensity further away from the middle area of the Turkana channel during JJAS season (BCC-ESM1, CAMS-CSM1-0, SAM0-UNICON, TaiESM1, MIROC6, NESM3, INM-CM4-8, and INM-CM5-0). This phenomenon indicates that while the winds begin to accelerate at mid-Turkana channel, the gain in wind speed is lesser in them.

The CMIP6 models which are a source of lower magnitudes of wind speeds at lower-atmosphere are of lower resolution. Considering that a TJ characterized by high wind speeds that decrease aloft result from acceleration within the Turkana channel, the disparities between the ERA5, and some of the CMIP6 models are likely to result from TJ interaction with topography within the channel.

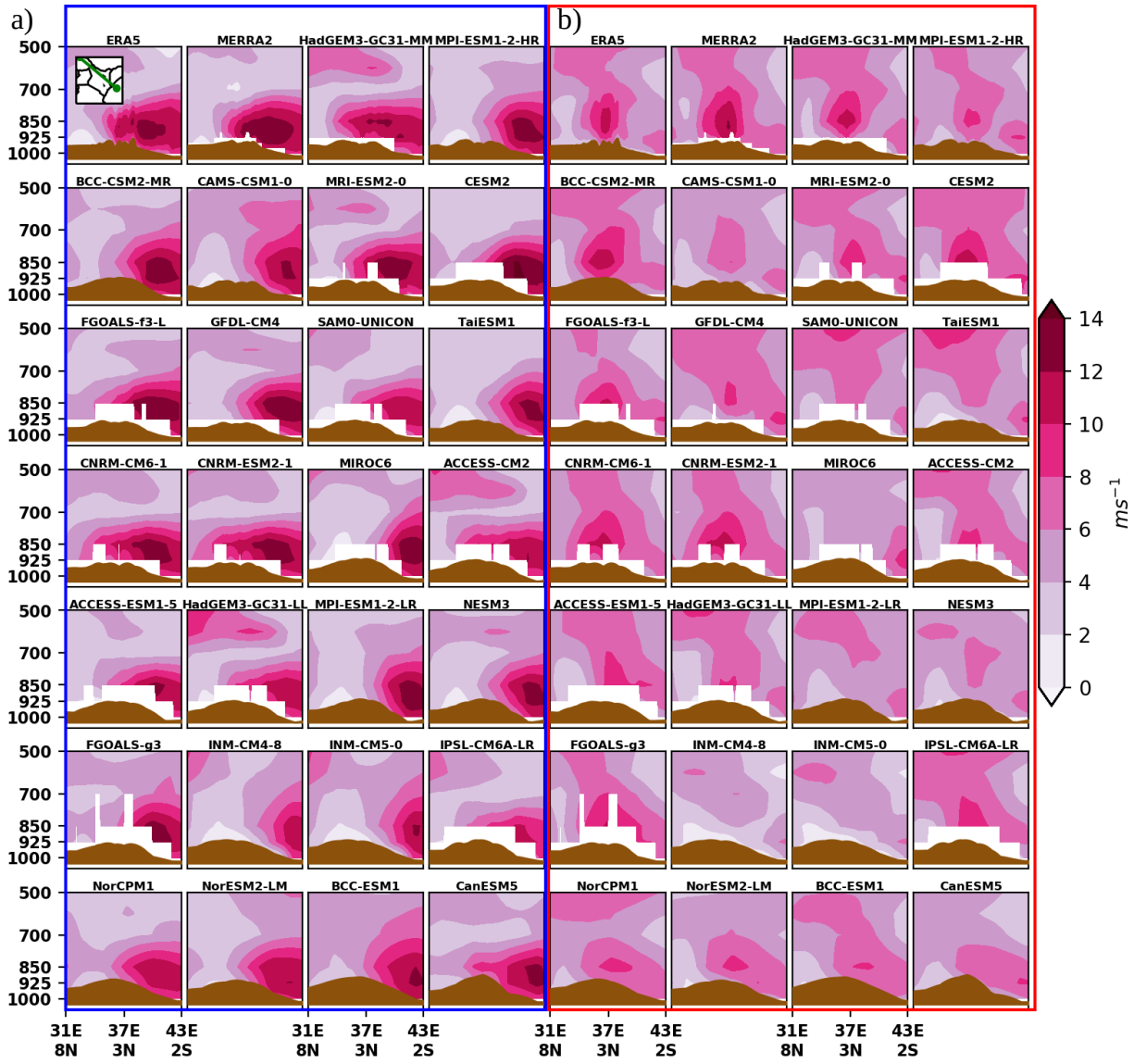

Figure 5. *Vertical cross-section of climatological mean wind speed (m/s) for June to September (left plot) and October to May (right plot) for the years 1980 to 2014. Cross-sections are drawn for transect parallel to Turkana channel in Northwest (31°E and 8°N) to Southeast (43°E and 2°S) direction. The transect is shown insert plot a-ERA5 subplot. Topography is illustrated in the bottom of each subplot in brown. Topography is illustrated in the bottom of each subplot.*

4.2.3 Mean vertical flow in the Turkana channel

Figure 6 shows the mean omega velocity through the study period, plotted for the northwest to southeast axis parallel to the Turkana channel. Other than in the HadGEM-GC31-LL and the two versions of CNRM model, descending motions dominate the entrance of Turkana channel during the JJAS season and the mid-channel area during the months of October to May in CMIP6 models. Relating these results with those in Figure 4 shows that descending motions dominate lower atmospheric levels where the intensity of the TJ is strong. The ERA5, HadGEM-GC31-LL and the two versions of CNRM model have relatively faster winds at mid-Turkana area during JJAS season following intense TJ core in the season.

Additionally, the influence of the elevated terrain is noticeable. In both the JJAS and October to May seasons, ascending motion emanates between the entrance and mid-channel area where the floor of Turkana channel begins depicting an elevation, due to frictional interaction of the wind with the sloping floor of the Turkana channel. During JJAS season the TJ core accompanied by subsidence aloft is further to the right of the mid-Turkana channel. This allows low-level ascents manifesting at the TJ entrance to incline towards the middle and exit area of the channel with height as generation of the ascents diminish as surface elevation slopes downwards at Turkana channel exit. This further strengthens uplifts at the exit area in the deep troposphere. During October to May months, the TJ core accompanied by subsidence aloft is at the mid-Turkana channel area. Thus, ascents from the TJ entrance area are inhibited from lateral movement towards the mid-Turkana area. At TJ exit, vertical motions are generated by deceleration of winds that leads to build up of pressure at lower atmosphere.

Other than the ERA5 and the two CNRM models, other CMIP6 models show stronger ascending motion apparently from enhanced blocked lower atmospheric flow at the mid-Turkana channel. The ERA5, HadGEM-GC31 and CNRM models depict unblocked flow through the channel with pockets of near surface descending motion associated with faster wind speeds at the mid-Turkana channel area. During the months of October to May, the mid-channel descents are stronger. This shows that although strong TJ intensity induces the subsidence in the Turkana channel, the interaction between the TJ and the Turkana channel influences the intensity of the TJ core.

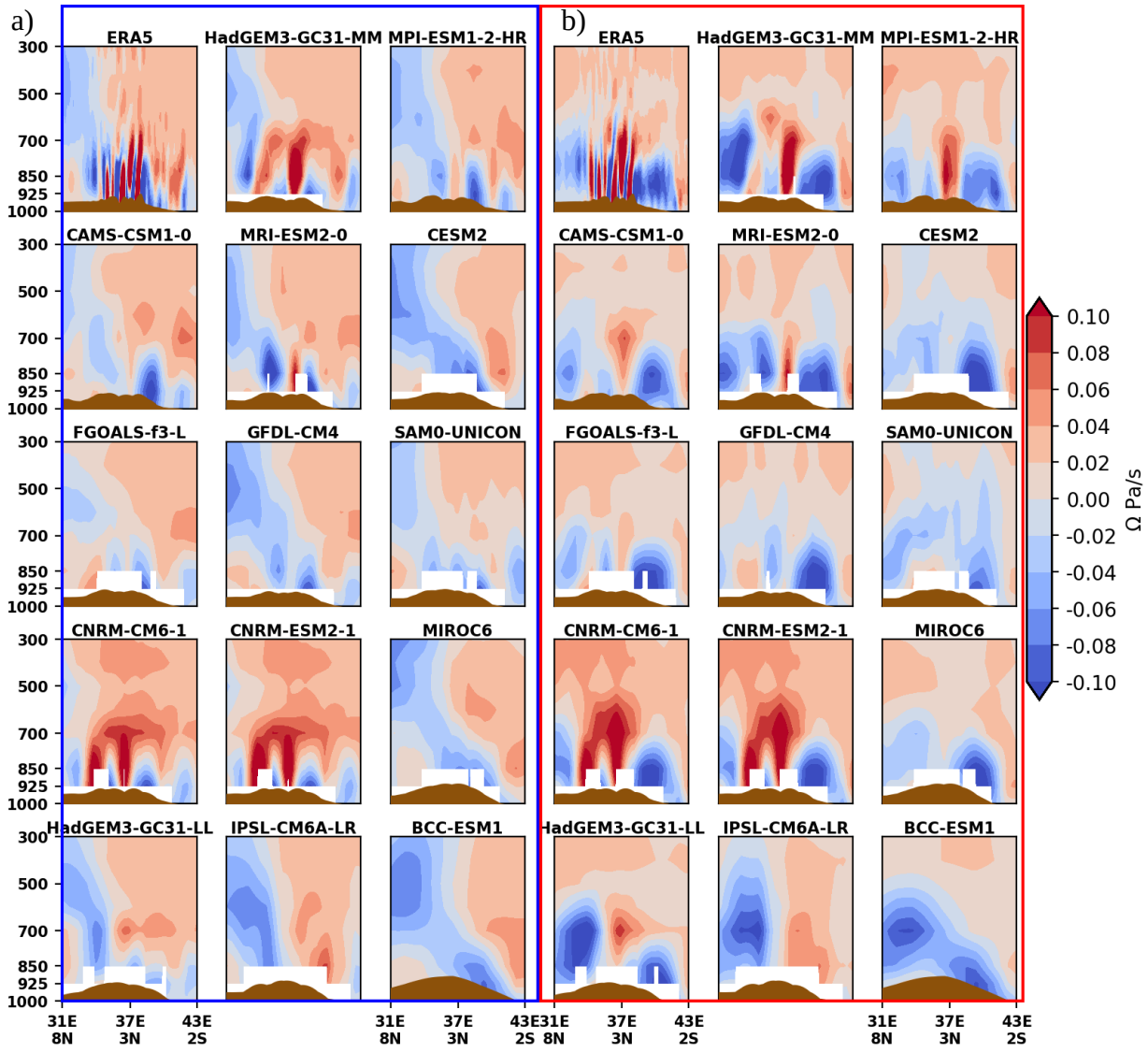

Figure 6. *Vertical cross-section of climatological mean omega (Pa/s) for June to September (left plot) and October to May (right plot) for the years 1980 to 2014. Cross-sections are drawn for transect parallel to Turkana channel in Northwest (31°E and 8°N) to Southeast (43°E and 2°S) direction, like that used to develop Figure 4. Topography is illustrated in the bottom of each subplot.*

4.3 Topographic influence on the TJ in CMIP6

4.3.1 Turkana channel in CMIP6

Figure 7a shows that the Turkana channel is the largest topographic feature below the 850 mb level within the study area bounded by longitudes 33°E and 41°E and latitudes 2°S and 9°N. The floor of the channel at the entrance is roughly 980 mb in ERA5 and the CMIP6 models. The channel floor rises gently and occupies a varied level of between 945 and 960 mb, matched with high walls of at 915 mb in the RA and the models with less than 1° grid step size. In coarser resolution models, the floor of the channel rises to higher level that is fairly similar, approximately at 930 mb. Therefore, the channel appears flattened in them. The CanESM5 and the BCC-ESM1 models have floor of the channel in them, higher above 850 mb.

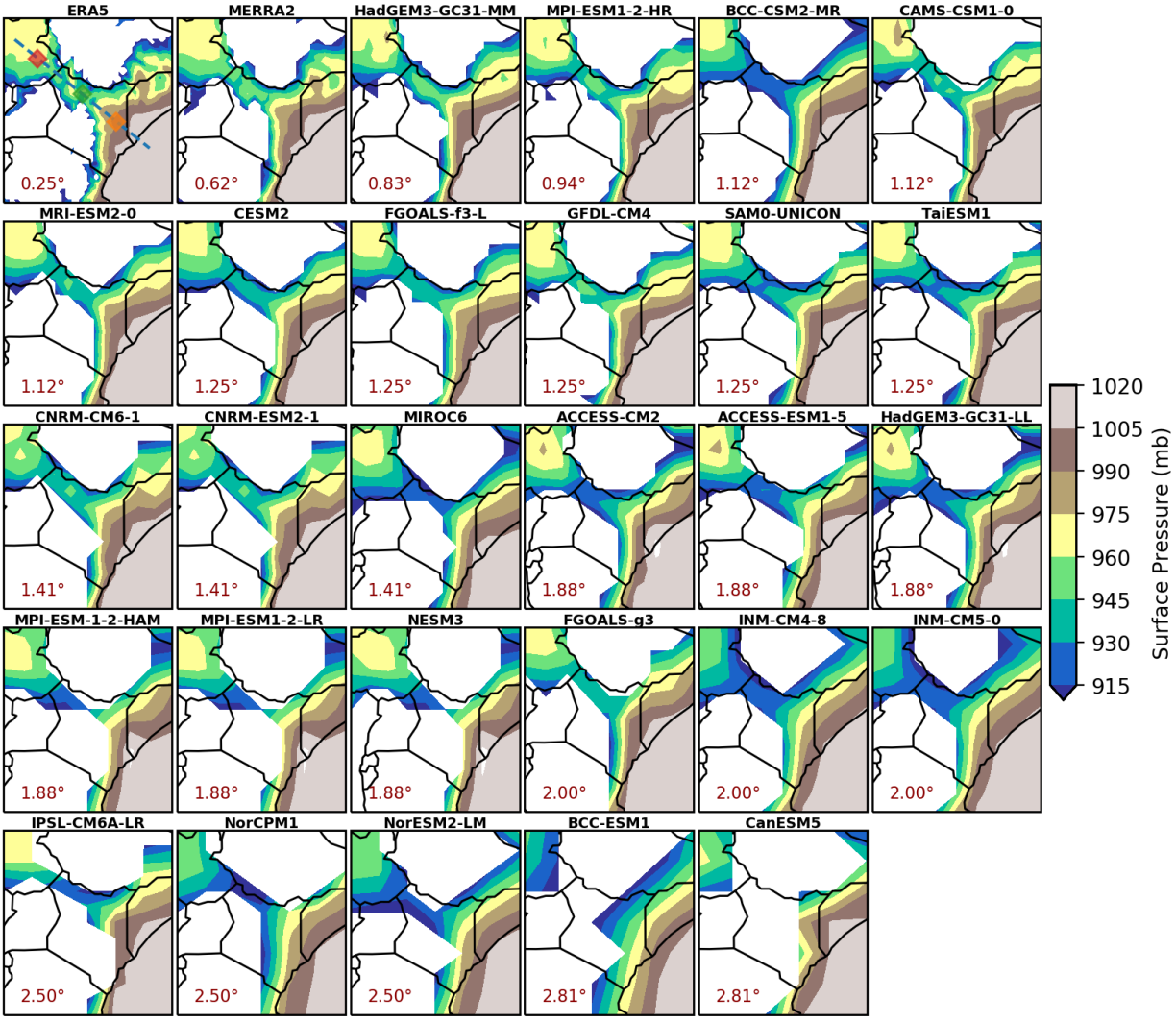

Figure 7a. *Surface elevation in ERA5 and the CMIP6 models over the Turkana channel area, with*

elevation above 850 mb level masked out. The in-plot texts indicate the model longitudinal grid step size. The blue dotted line in the ERA5 panel show a transect parallel to the Turkana Channel in Southeast (entrance; orange) to Northwest (exit; red) direction through a point at center of the channel (green; 37°E and 3°N). The area bordering Tanzania, Kenya and Somalia on their eastmost boundary, is below sea-level (1,000 mb) while white patches show elevation above 850 mb level.

Figure 7b shows the cross-section of the Turkana channel at each longitude. The channel narrows from about 700 square kilometers in the RA (ERA5 and MERRA2) and about 600 square kilometers in CMIP6 models at 41°E longitude within 2°S and 9°N latitudes. The models and the RA attain a restriction at 37°E, and the constriction is prominent in the RA plus about half of the models. The INM, NorCPM1 and NorESM2-LM models attain this constriction at 38°E. Exiting at the 37°E longitude. The channel widens to about 200 square kilometers further to the west of this longitude according to most of the models, other than the CanESM5 and the BCC-ESM1. The 2 models have an apparent exit of the channel at 35°E. Through the Turkana channel, the RA some models (HadGEM-GC31-MM, MPI-ESM1-2-HR, BCC-CSM2, CAMS-CSM1, MRI-ESM2, CESM2) exhibit a wider channel at 36°E. The feature becomes prominent when the model has a higher resolution. As such the ERA5 which has the highest resolution (0.25°) prominently shows the widening.

While the narrowing results in the formation of a constriction at the 37° E longitude, the changes between adjacent cross sections are varied in CMIP6 models compared to the consistency observed in ERA5, consistent with results in Vizy and Cook (2019). Other than the HadGEM3-GC31-MM and MPI-ESM1-HR models, cross-sectional areas at some adjacent longitudes are maintained or least changed. Strikingly, the CanESM5 exhibits higher changes whenever a difference is observed at its relatively coarse spatial grid resolution. The results from the ERA5 and the two high-resolution CMIP6 models show that reducing the grid-step size increases topographic details being resolved and forms a funnel-shaped Turkana channel. The narrowing phenomenon has been used to explain existence of a faster TJ in MERRA2 as it has a consistently narrowing channel (Vizy and Cook, 2019). The next step of this analysis explores how these finer details of the topography relates with the representation of the TJ.

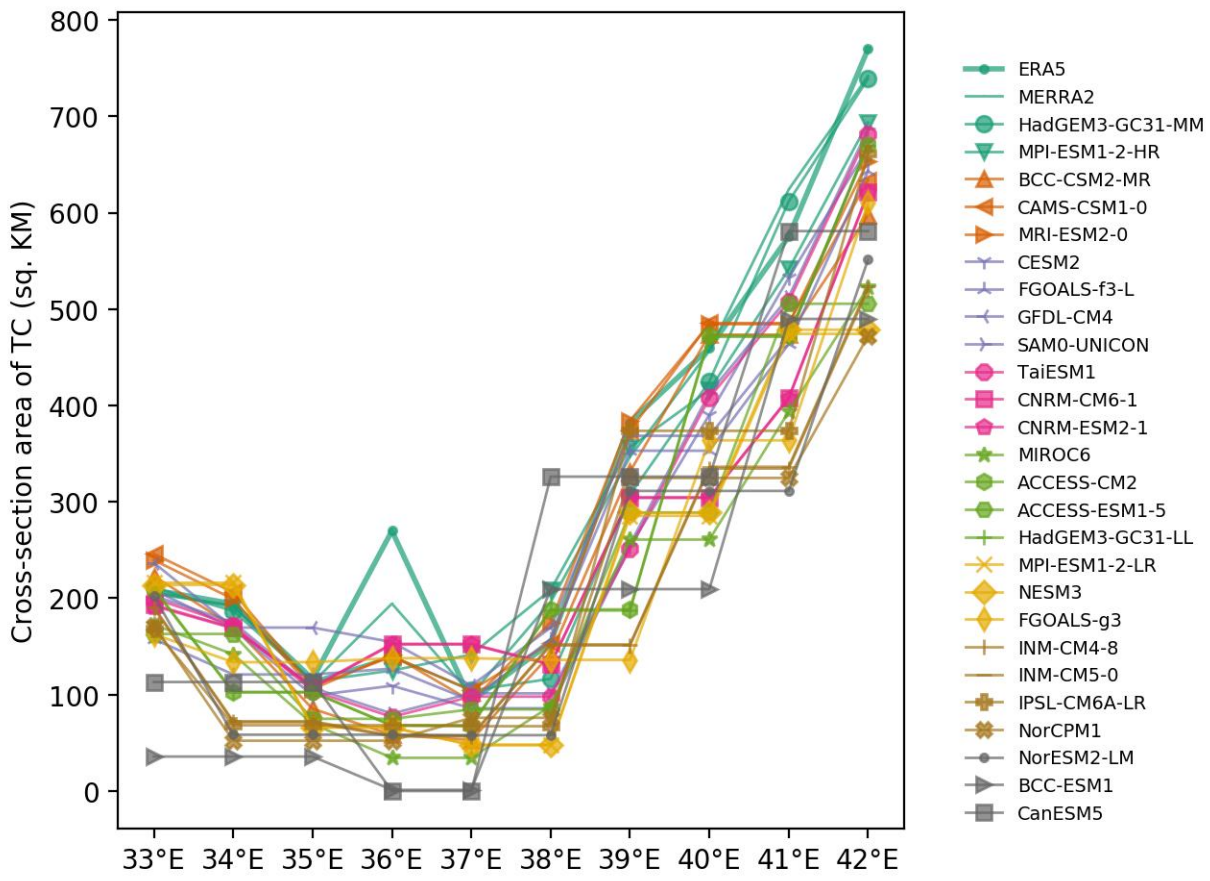

Figure 7b. *Estimated cross sectional area of Turkana Channel (in square kilometers) at each longitude between latitudes 2° S to 9° N. The quantity is abbreviated as TC.*

4.3.2 Relationship between TJ and Topography in historical AMIP

The difference between the cross-sectional area of the channel at the entrance and exit of the jet is computed. Figure 8 shows the narrowing index for CMIP6 models as well as the horizontal resolution (longitudinal grid step size) of the model. Since the cross-sectional area entrance of the channel (42°E) in the ERA5 and all the CMIP6 models is about 800 square kilometers and reduces to about an eighth of this at the mid-channel, models with zero changes between adjacent longitudes have higher gradient whenever shape changes. Thus, a low index (Figure 8, y-axis), which is characteristic of low-resolution models with higher grid step sizes, characterizes steep change in terrain followed by blocks of wall between the adjacent longitudes with constant cross-section area between them.

The ERA5 has the highest narrowing index for the Turkana channel. It is followed by CMIP6 models of less than 1.5° resolution in which the index is either maintained or weakens in models with higher grid-step sizes. At greater than 1.5° resolution, the CMIP6 models scattered values for the index and show inconsistency in how the narrowing of the channel is lost with increasing coarseness in the topography. The CanESM5 model is an outlier, returning a high value of the quantity due to high rates of change associated with very large grid-step sizes and a smaller number of points in the channel (Figure 8b). Therefore, linking this result with those from Figure 6 indicates that CMIP6 models with resolution greater than 1.5° have steep walls along the floor and height of the channel. This is a likely source of the impediment on the smooth flow near the surface along the Turkana channel.

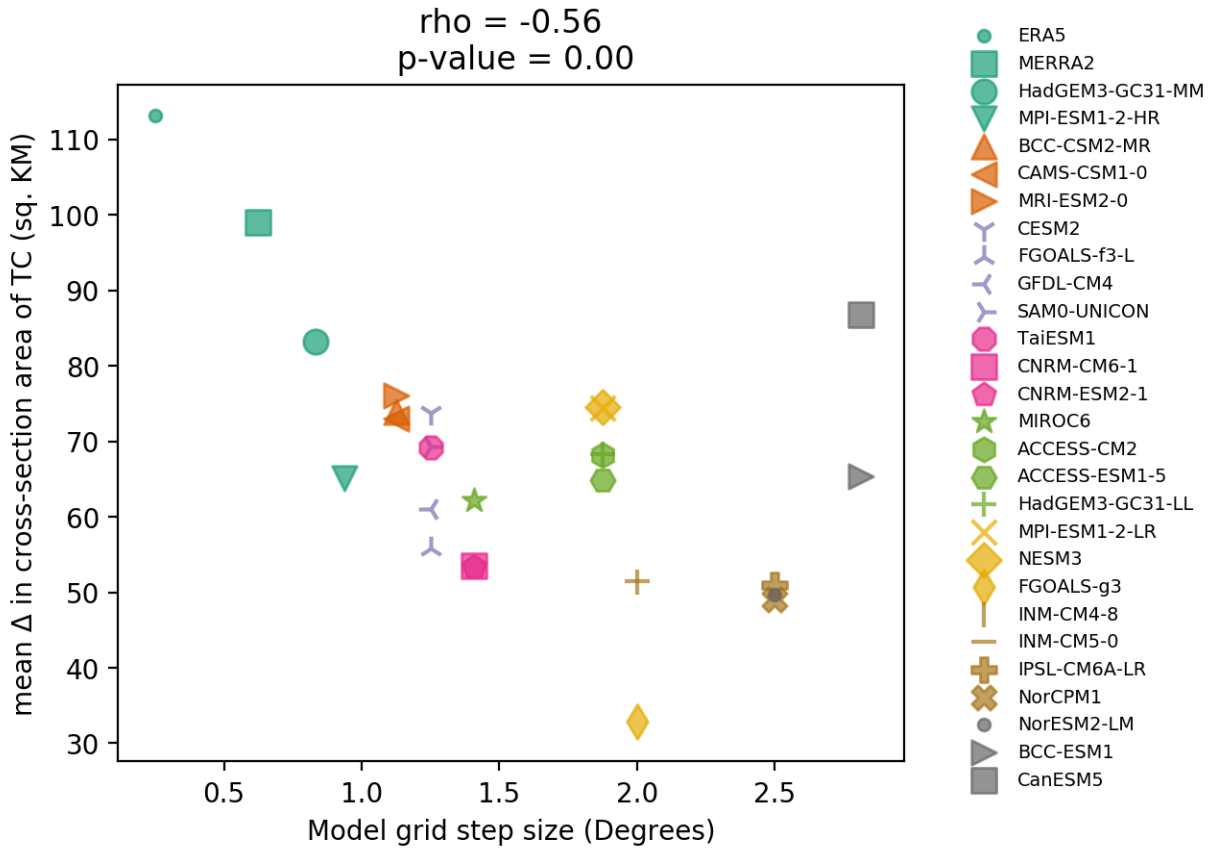

Figure 8. *Mean zonal change in cross-sectional area of Turkana channel estimated between longitudes 33° E and 42° E, each longitude spanning between latitudes 2° S to 9° N; referred to as the narrowing index in this paper. The quantity is computed for different models on their native*

grid whose longitude grid spacing are shown in the x-axis. The Pearson product moment correlation coefficient (rho) between the narrowing index and the horizontal grid resolution shows significant correlation at the 95% confidence level (p-value < 0.05)

The association between the strength of the TJ and the shape of the Turkana channel represented by the narrowing index, is explored in this section by adjusting the thresholds for JJAS season maximum wind speed and vertical shear (between the point of maximum and minimum wind speed before reaching 500 mb). Figure 9 shows TJ counts for wind speeds at 850 mb in range 6 to 10 m/s and wind "shear" above the TJ core in range 2 to 6 m/s, for each model and its narrowing index.

Most models return a TJ with maximum wind speeds exceeding 6 m/s and vertical wind shear above the TJ core exceeding 2 m/s. Only the CMIP6 models INM and ACCESS-ESM have the TJ structure weaker than this category within the 35-year study period. Higher thresholds of 9 m/s at 850 mb and vertical wind shear of 5 m/s TJs are still common in the majority (17) of the 26 CMIP6 models. At a level higher (9 m/s maximum wind speeds and greater than 6 m/s vertical shears above the TJ core), a robust positive correlation exists between the TJ counts and the narrowing index. At this point, the criteria are stricter and nearly half of the CMIP6 models return zero TJ counts. Therefore, we consider those thresholds as optimal.

The optimum thresholds are surpassed in CMIP6 models having a high index for the shape of the Turkana channel such as HadGEM3-GC31-MM, CNRM and MRI. This is similar to the ERA5 which has the highest index (Figure 7) considering TJs whose core is characterized by at least 9 m/s maximum wind speeds which decrease by at least 5 m/s above. Referring to Figure 4, the mean TJ in ERA5 reaches higher values for maximum wind speeds at 12 m/s, decreasing by 7 m/s above the core. But CMIP6 models with narrowing index exhibit mixed TJ characteristics. For instance, the CNRM and FGOALS-f3-L models exhibit TJs when NorESM2-LM and INM models of comparable index, return zero TJ count considering the optimum thresholds for the TJ in CMIP6 models. There were 9 CMIP6 models with zero TJs and 4 models with 35 TJs reaching the optimum threshold in 35 JJAS seasons. The remaining 13 CMIP6 models occasionally exhibited TJs reaching the optimum threshold for a strong jet (maximum wind speeds of 9 m/s and decreasing aloft the core by at least 5 m/s).

The different CMIP6 models (coarser than 1.5° longitudinal resolution) with low narrowing index show a lower consistency in narrowing cross sectional area. Considering that the narrowing supports channelling of the winds and acceleration of the winds (Indeje et al., 2001), models with coarser than 1.5° longitudinal grid step size which occasionally exhibit weak TJ structure, are here found to be related to poor resolution of the Turkana channel. These irregularities in the TJ strength could also influence rainfall at TJ exit, as the TJ is considered a moisture transport mechanism (Munday et al., 2020).

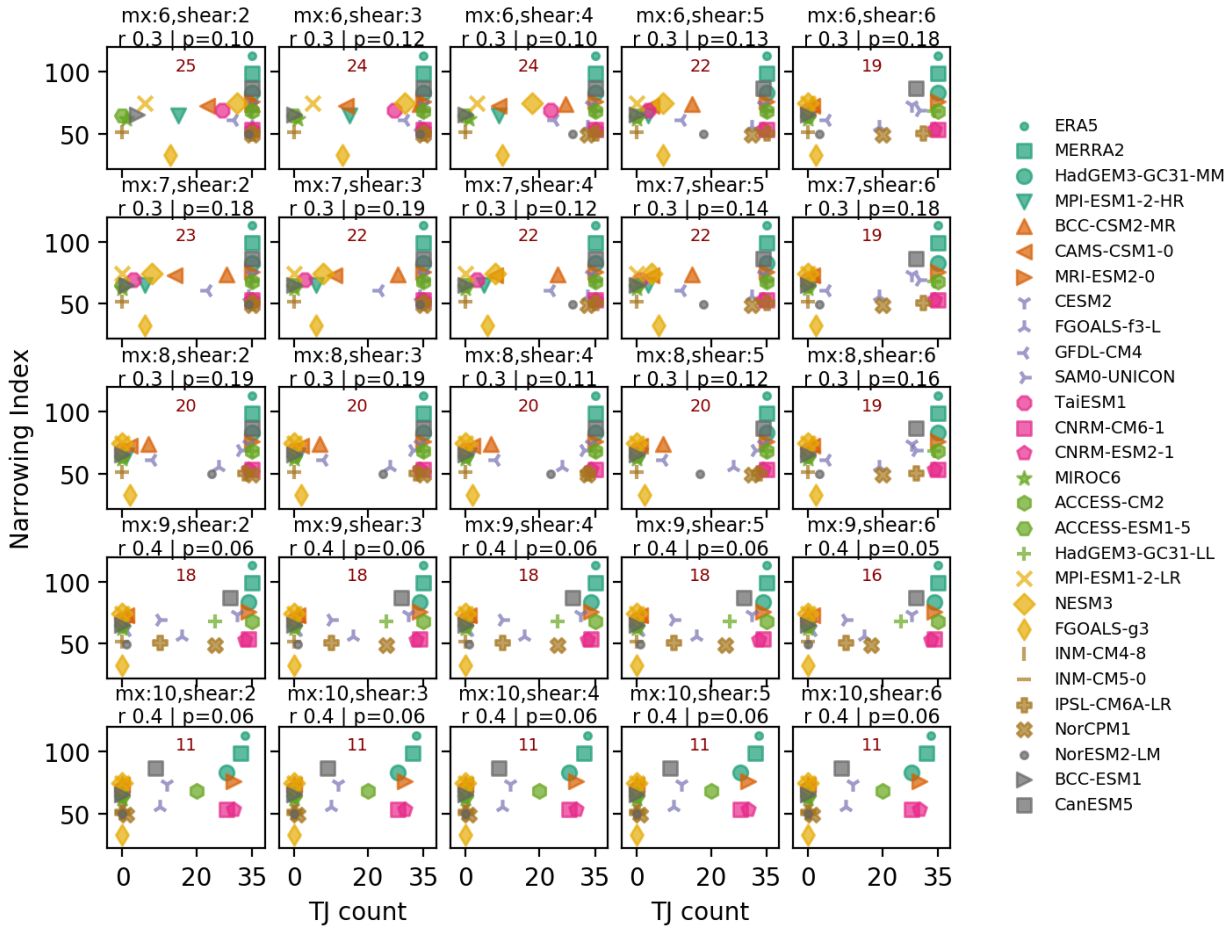

Figure 9. *Dependence of the TJ occurrence on the narrowing index. Counts are made for the TJ of maximum wind speeds and highest decrease between 850mb and point of minimum below 500 mb, shown in the title of each subplot. Also shown in text are spearman's rank correlation and p-value between TJ counts and narrowing index. The number of models returning more than zero (0) TJ count is shown in inner text*

4.4 Relationship between TJ and East African climate in CMIP6

The influence of the TJ on the climate of East Africa precipitation is investigated in the JJAS season for CMIP6 models having an irregular TJ (Figure 10). In the models, JJAS is a major season with rainfall accumulation of up to 1,100 mm over the northwest regions of East Africa, particularly over western of Ethiopian highlands. Other areas with similar precipitation amounts include Northern Congo, most of Central African Republic and the west of South Sudan in CanESM1 and lesser magnitude (900 mm) over these areas in GFDL, CESM2, HadGEM (both) MRI, NorESM1, NorCPM1, IPSL and SAM. In those models, areas that border exit of the TJ (northern Kenya boarder with South Sudan) have about 500 mm rainfall within this season, an area which has observed climatological annual rainfall of 700 mm, mainly received in JJAS (Camberlin, 2018). In the CAMS, FGOALS, and both versions of CNRM, the areas at immediate exit of the TJ and most of South Sudan, are drier with less than 300 mm precipitation during this season.

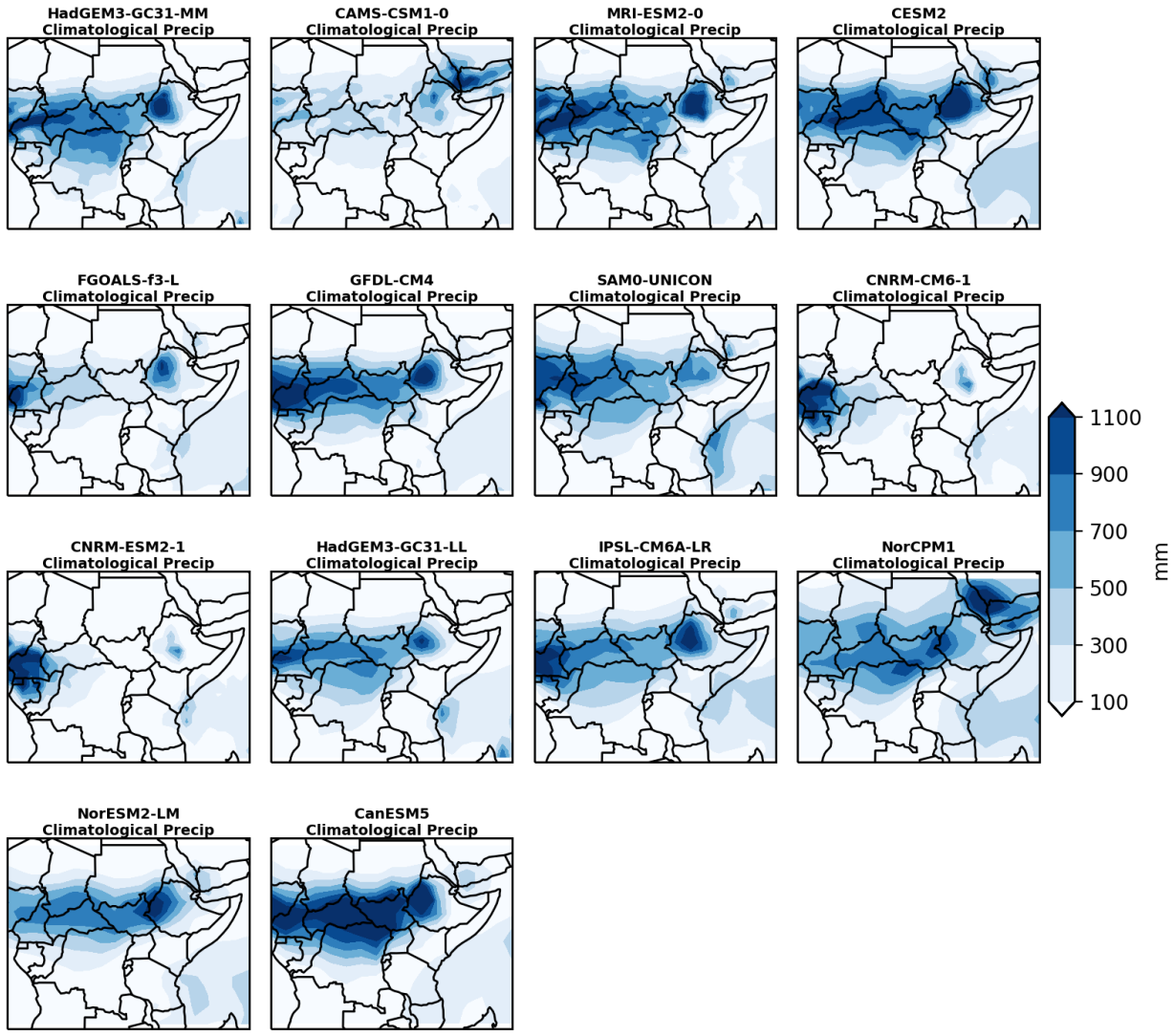

Figure 10. *Mean climatological precipitation during the June to September season for the years 1980 to 2014.*

The influence of the TJ on the model climate of East Africa in JJAS, is shown using the composite anomalies of precipitation associated with the TJ (Figure 11). Mean precipitation anomalies are shown for strong TJs in the CMIP6 models that best match TJ strength in the ERA5 (at least 9 m/s at the 850 mb and vertical wind shear of at least 5 m/s above TJ core) in the "jet" panel and also when the strength was weaker "no jet cases" panel. The climatological conditions of north-western of East Africa, are also mirrored when the TJ strength is regularly either strong or wet. Fluctuations

in the TJ strength which is common in nearly half of the CMIP6 models used, induce spatial distribution of dry and wet anomalies.

In Figure 11 both versions of CNRM have a regularly strong TJ. In them, high speed winds extend furthest into the channel (Figure 4) so although it is a high jet count model, it is wetter further west to other models (in Figure 10). The CanESM model equally a regularly strong TJ albeit the high-speed winds do not extend as much compared with CNRM into the channel (Figure 4) so it is wetter from the immediate exit of the TJ compared to other models (in Figure 10). Left panel of Figure 11 shows anomalies associated with the TJ. When a perennially weak TJ strengthens in model climatology, dry anomalies at the border region of the exit the Turkana channel are exhibited. Specifically, rainfall is suppressed by up to 200 mm below the climatological mean, exhibited in CAMS, BCC, GFDL and FGOALS. The dryness extends up to the west of South Sudan, east of Central African Republic, northern Congo and to the west of Ethiopian Highlands. The increasing dry anomalies at the TJ exit area is associated with stronger inflow of air with low moisture content during this season through lower atmosphere. Furthermore, during a strong TJ, easterly flow is so strong that it inhibits south-westerly advection of moist air from equatorial Congo.

Conversely, wet anomalies characterize the immediate exit of Turkana channel and Ethiopian highlands in the CMIP6 models when perennially strong TJ weakens below the thresholds (Figure 11; right panel). Precipitation is enhanced by up to 200 mm more than the climatological mean in the models. Further to the west of South Sudan, in the Central African Republic and northern Congo, dry anomalies below the climatological mean are exhibited. This is likely associated with enhanced uplift of moist air that is transported from the Indian Ocean through the Turkana channel at TJ exit. In this case, pressure piles up at the immediate exit due to deceleration of winds and promotes zonal advection of moisture-laden air to the western regions of South Sudan (Vizy and Cook 2019). Furthermore, during a weak TJ, south-westerly advection of moist air from equatorial Congo is likely being promoted.

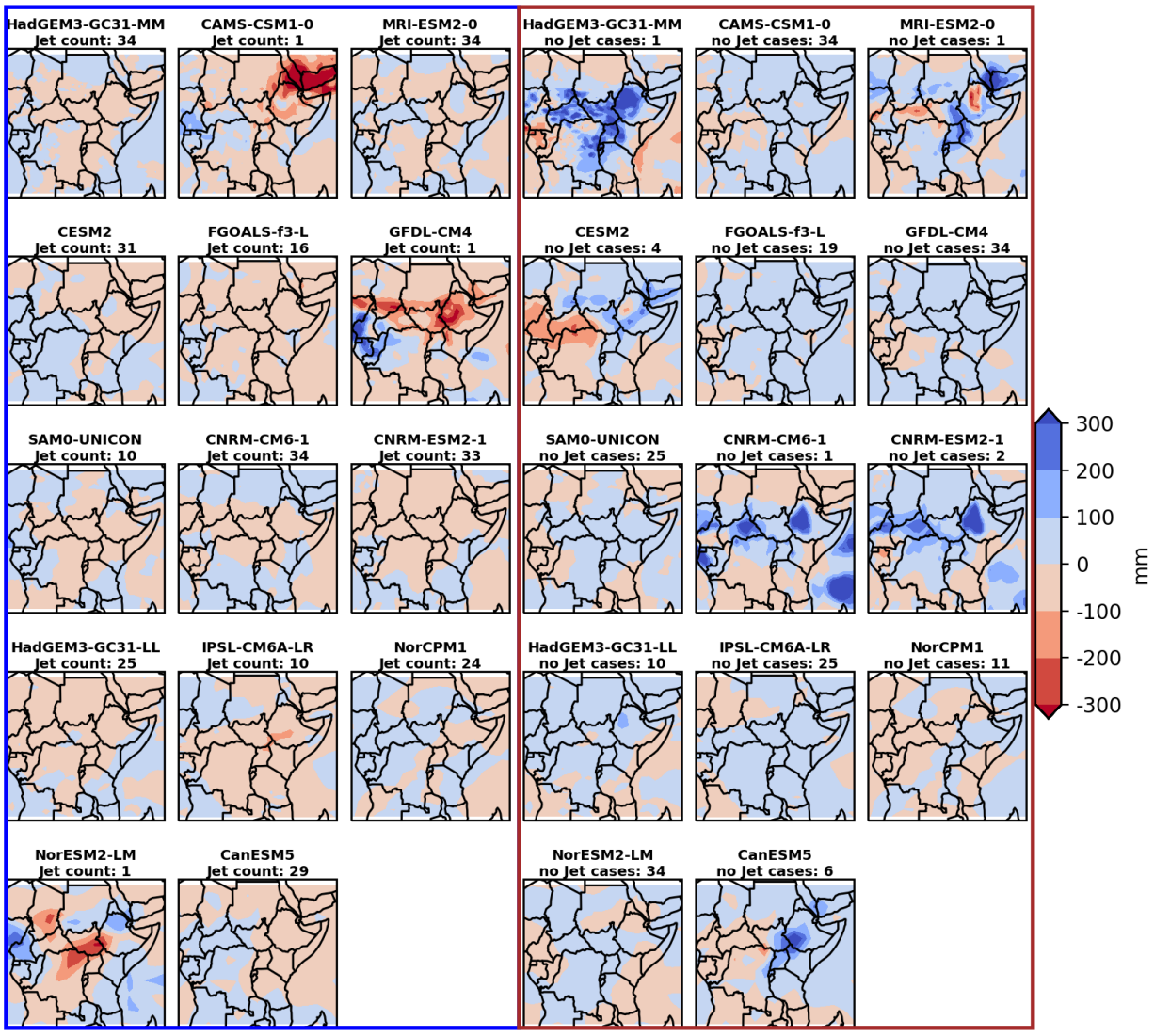

Figure 10. *Composite anomalies for precipitation during the June to September season for the years 1980 to 2014. Left panel shows the composite anomalies for jet occurrence (TJ core speeds at least 9 m/s and decreases above the core by at least 5 m/s; JJAS seasons in which thresholds were met). Right panel shows the composite anomalies for no jet occurrence (TJ core speeds at least 9 m/s and decreases above the core by at least 5 m/s; JJAS seasons in which thresholds were not met)*

CHAPTER FIVE

SUMMARY, CONCLUSIONS AND RECOMMENDATIONS

5.1 Introduction

This chapter provides a summary of the study, key results and major conclusions drawn from the results of the study. It also provides some recommendations for applications of the study findings and suggestions for future studies.

5.2 Summary

The TJ is a persistent jet stream that is observed throughout the year in the ERA5 data with wind speeds ranging between 11 m/s and 13 m/s at approximately 850 mb level. However, it varies appreciably with typical core speeds ranging between 5 and 9 m/s in CMIP6 models. The maximum wind speed at the core of the TJ in both the ERA5 and the HadGEM-GC31-LL model is highest during June to September, a feature that is not captured by the majority of the CMIP6 models, which show their minimum wind speeds in the season.

The period from June to September is characterized by strongly decreasing winds above the TJ core at the mid-Turkana channel and the presence of the EALLJ in both the ERA5 and CMIP6 models. When the EALLJ is present, the models show high wind speeds (up to 9 m/s) closer to the entrance of the Turkana channel while the winds at the mid-channel area slow down up to 5 m/s. This indicates that the TJ is merged with the EALLJ, which obscures the strong winds towards the mid-Turkana channel. In the absence of the EALLJ, the high wind speeds associated with TJ core in CMIP6 models (up to 9 m/s) shift northwestwards to the mid-Turkana channel area. Furthermore, the core of the TJ appears vertically extended up to 700 mb in the models and reduces the magnitude of change between maximum wind speed at TJ core and minimum wind speeds found aloft at the mid-channel. The vertical wind profiles are therefore mixed in most CMIP6 models.

Analysis of vertical winds indicate that the mixed profiles of wind speed in the CMIP6 models is potentially related to ascending motion from the mid-Turkana channel that leads to the upward spread of relatively high wind speeds. The upward flow from the mid-channel could be enhanced

by frictional interaction with the floor and wall of the Turkana channel and is pronounced in CMIP6 models with horizontal resolution of coarser than 1.5°. The frictional encounter of the wind flow with the floor of the Turkana channel appears as enhanced ascending motion from blocked flow at mid-Turkana channel. The enhanced ascent due to blocked motion is likely to result in heightening of precipitation. From this analysis, precipitation is enhanced up to 200 mm in the season at exit of the TJ by the ascents in CMIP6 models with longitudinal grid step size higher than 1.5°.

5.3 Conclusions

This study provides insights on the representation of features of the TJ in the available CMIP6 models and ERA5 dataset. The results also reaffirm the importance of the TJ to the climate of East Africa by transporting moisture during the northern summer, an aspect also presented in other studies including Indeje *et al.*, (2001), Nicholson (2016), Vizy and Cook (2019) and King *et al.*, (2021). Additionally, we find that higher resolution CMIP6 models have a better Turkana channel characterized by consistent narrowing along the channel (through the narrowing index) which allows for smooth flow and acceleration of winds at mid-Turkana channel area. The study has demonstrated that for coarse model resolution with a low of at least 1.5°, the narrowing index is low and produces a TJ with high variability in its strength, location of core and vertical structure. The variation in strength, location and structure of the TJ translates to biases in the CMIP6 model rainfall climatology over Eastern Africa, leading to emergence of dry (wet) anomalies over the north-western region of East Africa when the TJ is strong (weak). The enhancement of wet anomalies is up to 400 mm above the observed climatology at the immediate exit of the TJ when the jet stream is weaker. The area of influence of the TJ boarders the drier Sudan to the north, whose annual precipitation, mainly from the JJAS season is lower than 400 mm. Therefore, the TJ is likely to be critical to the climate regime in the relatively wetter areas of northwestern of East Africa, as well as the drier climate of the surrounding.

5.4 Recommendation

These findings demonstrate the importance of realistically representing the topography details over the Turkana channel based on an analysis using model data. This highlights the need for field studies to determine a realistic baseline for comparison of the observed climatology of the TJ and

the relationship between the TJ and rainfall. While an understanding of the TJ features can be drawn from some low-resolution RA and models (e.g., Nicholson 2016, King *et al.*, 2021), most of them have high variability in seasonal cycle in strength of the TJ in models, which is not being exhibited in the closest to observations dataset. This implies that model information could mislead if used for planning using the wind data. There is still need to postprocess wind and rainfall data from the models over the northern Kenya area especially Turkana channel to remove biases as the TJ provides potential for wind energy, which the government can invest in to supplement energy of sources. There is also the need for increased resolution to realistically represent the TJ. The narrowing index provides a quantitative way to track improvement of high-resolution modelling to the narrowing shape of the Turkana channel, much needed to realistically represent the structure, position, strength of TJ and influence on rainfall in atmospheric models. The next steps for this work are to apply our findings to models with resolution hierarchy in controlled experiments and further explore the factors responsible for the inter-annual variability of the perennially weak TJ in the CMIP6 models.

REFERENCES

Acosta, R. P., and Huber, M. (2017). The neglected Indo-Gangetic Plains low-level jet and its importance for moisture transport and precipitation during the peak summer monsoon. Geophysical Research Letters, 44(16), 8601–8610. doi:10.1002/2017gl074440

Ba M.B, Nicholson S.E (1998). Analysis of convective activity and its relationship to the rainfall over the Rift Valley lakes of East Africa during 1983-1990 using the METEOSAT infrared channel. J. Clim. Appl. Meteorol. 10: 1250–1264.

Eyring, V., Bony, S., Meehl, G. A., Senior, C. A., Stevens, B., Stouffer, R. J., and Taylor, K. E. (2016). Overview of the Coupled Model Intercomparison Project Phase 6 (CMIP6) experimental design and organization, Geosci. Model Dev., 9, 1937–1958, https://doi.org/10.5194/gmd-9-1937-2016.

Hart J. E, Rao G.V, Van De Boogaard H, Young J.A, Findlater J. (1978). Aerial observations of the East African low-level jet stream. Mon Weather Rev 106(12):1714–1724

Hartman A. T (2018) An analysis of the effects of temperatures and circulations on the strength of the low-level jet in the Turkana Channel in East Africa. Theor Appl Climatol 132:1003–1017. https://doi.org/10.1007/s00704-017-2121-x

Hersbach, H., Bell, B., Berrisford, P., Hirahara, S., Horányi, A., Muñoz-Sabater, J., Nicolas, J., Peubey, C., Radu, R., Schepers, D., Simmons, A., Soci, C., Abdalla, S., Abellan, X., Balsamo, G., Bechtold, P., Biavati, G., Bidlot, J., Bonavita, M., De Chiara, G., Dahlgren, P., Dee, D., Diamantakis, M., Dragani, R., Flemming, J., Forbes, R., Fuentes, M., Geer, A., Haimberger, L., Healy, S., Hogan, R.J., Hólm, E., Janisková, M., Keeley, S., Laloyaux, P., Lopez, P., Lupu, C., Radnoti, G., de Rosnay, P., Rozum, I., Vamborg, F., Villaume, S., Thépaut, J.N., (2020). The ERA5 global reanalysis. Q. J. R. Meteorol. Soc. 146 (730). https://doi.org/10.1002/qj.3803.

Hufman G.J, Adler R.F, Bolvin D.T, Gu G, Nelkin EJ, Bowman KP, Hong Y, Stocker EF, Wolf D.B (2007). The TRMM multisatellite precipitation analysis (TMPA): quasi-global, multiyear, combined-sensor precipitation estimates at fine scales. J Hydrometeorol 8:38–55. https://doi.org/10.1175/JHM560.1

Indeje M, Semazzi F.H.M, Xie L, Ogallo L.J, (2001). Mechanistic model simulations of the East African climate using NCAR regional climate model: influence of large-scale orography on the Turkana low-level jet. J. Clim. 14: 2710–2724

James, R., R. Washington, B. Abiodun, G. Kay, J. Mutemi, W. Pokam, N. Hart, G. Artan, and C. Senior, (2017). Evaluating climate models with an African lens. Bull. Amer. Meteor. Soc. doi:10.1175/BAMS-D-16-0090.1, in press.

Kilavi, M., MacLeod, D., Ambani, M., Robbins, J., Dankers, R., Graham, R., Todd, M. (2018). Extreme Rainfall and Flooding over Central Kenya Including Nairobi City during the Long-Rains Season 2018: Causes, Predictability, and Potential for Early Warning and Actions. Atmosphere, 9(12), 472. doi:10.3390/atmos9120472

King, J. A., Engelstaedter, S., Washington, R., Munday, C. (2021). Variability of the Turkana low-level jet in reanalysis and models: Implications for rainfall. Journal of Geophysical Research: Atmospheres, 126, e2020JD034154. https://doi.org/10.1029/2020JD034154

Kinuthia J.H (1992). Horizontal and vertical structure of the Lake Turkana Jet. J. Appl. Meteorol. 31: 1248–1274.

Kinuthia J. H, Asnani G.C. (1982). A newly found jet in North Kenya (Turkana Channel). Mon. Weather Rev. 10: 1722–1728.

Krishnamurti, T. N., J. Molinari, and H. L. Pan (1976). Numerical simulation of the Somali jet. J. Atmos. Sci., 33, 2350–2362.

Levin N.E, Zipser E.J, Cerling T.E (2009). Isotopic composition of waters from Ethiopia and Kenya: insights into moisture sources for eastern Africa. J Geophys Res 114: D23306. https://doi.org/10.1029/2009JD012166

Liu M, Westphal D.L, Holt TR, Xu Q, (2000). Numerical simulation of a low-level jet over complex terrain in southern Iran. Mon. Weather Rev. 128: 1309–1327.

McCann, J. C, (1995). People of the plow: An agricultural history of Ethiopia, 1800–1990. Milwaukee, WI: University of Wisconsin Press.

Mekonnen A, Thorncroft C.D, (2016). On mechanisms that determine synoptic time scale convection over East Africa. Int J Climatol 36:4045–4057. https://doi.org/10.1002/joc.4614

Mukabana J. R and Pielke R. A (1996) Investigating the influence of synoptic-scale monsoonal winds and mesoscale circulations on diurnal weather patterns over Kenya using a mesoscale numerical model. Mon Weather Rev 124:224–242. https://doi.org/10.1175/15200493(1996)124%3c0224:ITIOSS%3e2.0.CO;2

Nicholson S. E. (1996) A review of climate dynamics and climate variability in eastern Africa. In The Limnology, Climatology and Paleoclimatology of the East African Lakes, Johnson TC, Odada E.O (eds). Gordon and Breach: Toronto, Canada, 25–56

Nicholson, S. E., (2014). The predictability of rainfall over the Greater Horn of Africa. Part I. Prediction of seasonal rainfall. J. Hydrometeorol., 33, 1011-1027, doi: 10.1175/JHM-D1129 13-062.1.

Nicholson S. E., (2016) The Turkana low-level jet: mean climatology and association with regional aridity. Int J Climatol 36:2598–2614. https://doi.org/10.1002/joc.4515

Njenga M., Leeuw J., O'Neill M., Ebanyat P., Kinyanjui M., Kimeu P., Adirizak H., Sijmons K., Vrieling A., Malesu M., Oduor A., and Dobie P. (2014). The need for resilience in the drylands of Eastern Africa. In Leeuw J., Njenga M., Wagner B., and Iiyama M (Ed) Treesilience: An Assessment of the Resilience Provided by Trees in the Drylands of Eastern Africa. World Agroforestry Centre Nairobi. DOI:10.13140/2.1.4118.5927

Ongoma, V., Chen, H., and Gao, C. (2017). Projected changes in mean rainfall and temperature over East Africa based on CMIP5 models. International Journal of Climatology, 38(3), 1375–1392. doi:10.1002/joc.5252

Otieno, V. O. and R. O. Anyah (2013). CMIP5 simulated climate conditions of the Greater Horn of Africa (GHA). Part II: projected climate. Clim. Dyn., 41 (7-8), 2099–2113, doi: 405 10.1007/s00382-013-1694-z.

Parry, J.; Echeverria, D.; Dekens, J. (2012). Maitima, J. Climate Risks, Vulnerability and Governance in Kenya: A Review; UNDP: New York, NY, USA, 2012; 78p. Available online:

https://www.iisd.org/system/files/publications/climate_risks_kenya.pdf?q=sites/default/files/publications/climate_risks_kenya.pdf (accessed on 3 August 2021).

Patwardhan, S., Kulkarni, A. and Sabade, S. (2016). Projected Changes in Semi-Permanent Systems of Indian Summer Monsoon in CORDEX-SA Framework. American Journal of Climate Change, 5, 133-146. http://dx.doi.org/10.4236/ajcc.2016.52013

Philip, S., S.F. Kew, G.J. van Oldenborgh, F. Otto, S. O'Keefe, K. Haustein, A. King, A. Zegeye, Z. Eshetu, K. Hailemariam, R. Singh, E. Jjemba, C. Funk, and H. Cullen. (2018). Attribution analysis of the Ethiopian drought of 2015. Journal of Climate 31 (6): 2465–2486. https://doi.org/10.1175/JCLI-D-17-0274.1.

Sun L.Q, Semazzi F.H.M., Giorgi F., Ogallo L. (1999) Application of the NCAR regional climate model to eastern Africa – 1. Simulation of the short rains of 1988. J. Geophys. Res. Atmos. 104: 6529–6548.

Taylor, K. E., Stouffer, R. J., and Meehl, G. A. (2012) An overview of CMIP6 and the experimental design, B. Am. Meteorol. Soc., 93, 485–498, https://doi.org/10.1175/BAMS-D-11-00094.1

Trewartha GT. (1981) The Earth's Problem Climates. University of Wisconsin Press: Madison, WI, 340 pp.

Uhe, P., Philip, S., Kew, S., Shah, K., Kimutai, J., Mwangi, E., Jjemba, E., (2018). Attributing drivers of the 2016 Kenyan drought. Int. J. Climatol. 38, 554–568.

Vizy, E. K., Cook, K.H. (2019) Observed relationship between the Turkana low-level jet and boreal summer convection. Clim Dyn 53, 4037–4058. https://doi.org/10.1007/s00382-019-04769-2

Williams A. P, Funk C, Michaelsen J, Rauscher S. A, Robertson I, Wils T. H. G, Koprowski M, Eshetu Z, Loader N. J (2012). Recent summer precipitation trends in the Greater Horn of Africa and the emerging role of Indian Ocean Sea surface temperature. Clim Dyn 39:2307–2328. https://doi.org/10.1007/s00382-011-1222-y

Yang, W., Seager, R., Cane, M. A., and Lyon, B. (2015). The Rainfall Annual Cycle Bias over East Africa in CMIP5 Coupled Climate Models. Journal of Climate, 28(24), 9789–9802. doi:10.1175/jcli-d-15-0323.1